Chapter 25

Numerical Simulation of Fully Grouted Rock Bolts

Hossein Jalalifar and Naj Aziz

Additional information is available at the end of the chapter

http://dx.doi.org/10.5772/48287

1. Introduction

This chapter describes the application of numerical modelling to civil and mining projects, particularly rock bolting, developing a Final Element (FE) model for the bolt, grout, rock, and two interfaces under axial and lateral loading, verifying the model, analysing the stress and strains developed in the bolt and surrounding materials.

Numerical methods are the most versatile computational methods for various engineering disciplines because a structure is discritised into small elements and the constitutive equations that describe the individual elements and their interactions are constructed. Finally, these numerous equations are solved together simultaneously using computers. The results from this procedure include the stress distribution and displacement pattern within a structure. Numerical modelling includes analytical techniques such as finite elements, boundary elements, distinct elements, and other numerical approaches that depend upon the material. The finite element method "FEM" is considered to evaluate the behaviour of materials and their interactions in a fully grouted bolt which is installed in a jointed rock mass. The simulations were carried out by ANSYS code.

2. FE in ANSYS

ANSYS is a powerful non-linear simulation tool, *Bhashyam.G.R* (2002).The ANSYS software is a commercial FE analysis programme, which has been in use for more than thirty years, *Pool et al.* (2003). The software can analyse the stress and strain built up in a variety of problems, especially designing roof bolts and long wall support systems.

The original code developed around a direct frontal solver has been expanded over the years to include full featured pre and post processing capabilities which support a

comprehensive list of analytical capabilities including linear static analysis, multiple non-linear analyses, modal analysis, contact interface analyses and many other types.

In this chapter only structural analysis is considered. Structural analyses are available in the ANSYS Multiphysics, ANSYS Mechanical, ANSYS Structural, and ANSYS Professional programmes only. Statistical analysis is used to determine displacement and stress and strain under static loading conditions (both linear and non-linear statistical analyses). Non-linearity can include plasticity, stress stiffening, large deflection, large strain, hyper-elasticity, contact surfaces, and creep behaviour.

3. A review of numerical modelling in rock bolts

A number of computer programmes have been developed for modelling civil and geo-technical problems. Some of them can be partially used to design and analyse roof bolting systems. It is noted that 3D software is necessary to simulate the whole characters of a model, such as modelling the joints, bedding planes, contact interface and failure criterion. Several numerical methods are used in rock mechanics to model the response of rock masses to loading and unloading. These methods include the method (FEM), the boundary element method (BEM), finite difference method (FDM) and the discrete element method (DEM).

A number of studies were carried out on bolt behaviour in the FE field, including those by *Coats and Yu* (1970), *Hollingshead* (1971), *Aydan* (1989), *Saeb and Amadei* (1990), *Aydan and Kawamoto* (1992), *Swoboda and Marence* (1992), *Moussa and Swoboda* (1995), *Marence and Swoboda* (1995), *Chen et al*. (1994, 1999, 2004), and *Surajit* (1999).

One of the earliest attempts to use standard FEs to model the bolt and grout was done by *Coats and Yu* (1970). The study was carried out on the stress distribution around a cylindrical hole with the FEmodel either in tension or compression. It was found that the stress distribution was a function of the bolt and rock moduli of elasticity. The presence of grout between the bolt and the rock was not considered and there was no allowance for yielding. The analysis was only carried out in linear elastic behaviour with two-phase materials, which limited the model. *Hollingshead* (1971) solved the same problem using a three phase material (bolt-grout and rock) and allowed a yield zone to penetrate into the grout using an elastic, perfectly plastic criterion, according to the Tresca yield criterion, for the three materials (Figure 1). How the interface behaved was not considered in the model.

John and Dillen (1983) developed a new one-dimensional element passing through a cylindrical surface to which elements representing the surrounding material are attached (Figure 2). They considered three important modes of failure for fully grouted bolts, a bi-linear elasto-plastic model for axial behaviour, elastic- perfectly plastic, and residual plastic model for bonding material, was assumed. Although this model eliminated many previous limitations and agreed with the experimental results, it neglected rock stiffness and in-situ stress around the borehole. They claimed that critical shear stress occurred at the grout - rock interface, which is not always the case in the field or laboratory. Aydan (1989) presented a FE model of the bolt. He assumed that a cylindrical bolt and grout annulus is connected to the rock with a three-dimensional 8-nodal points.

Two nodes are connected to the bolt and six to the rock mass. The use of boundary element and FE techniques to analyse the stress and deformation along the bolt was conducted by Peng and Guo (1992) (Figure 3). The effect of the face plate was replaced by a boundary element. The effect of reinforcement because of the assumption of perfect bonding was overestimated.

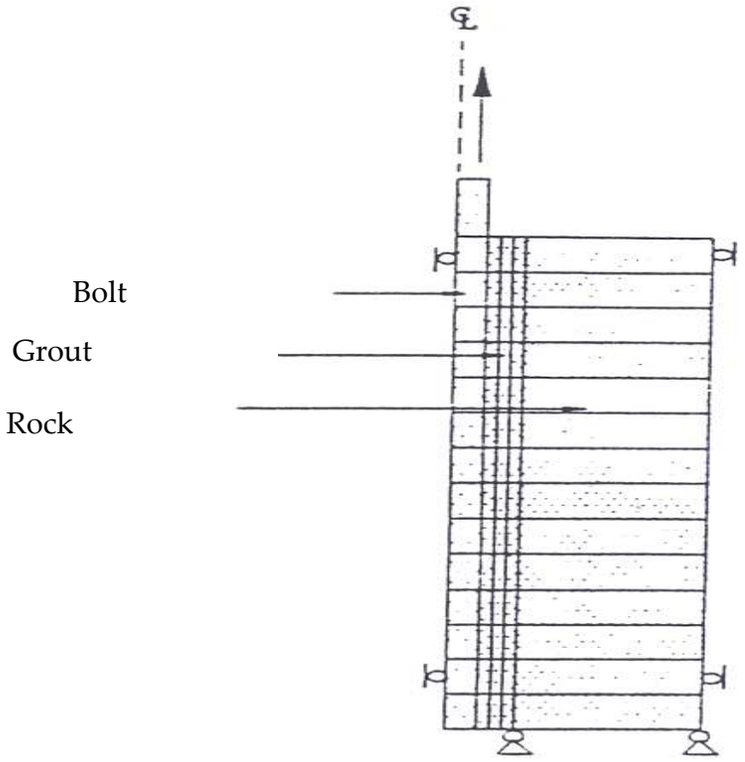

Figure 1. FE Simulation of bolted rock mass (after Hollingshead, 1971)

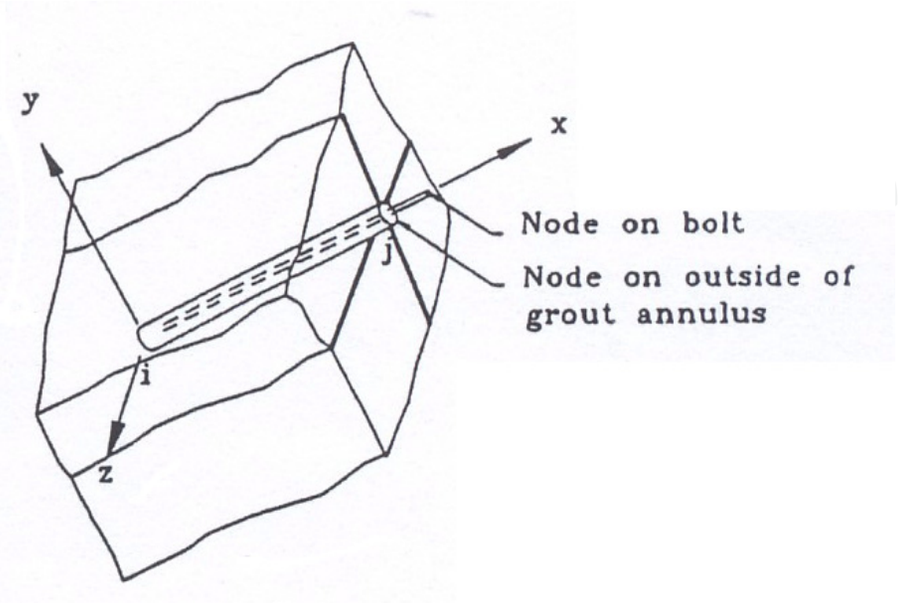

Figure 2. Three-Dimensional rock bolt element (after John and Dillen, 1983)

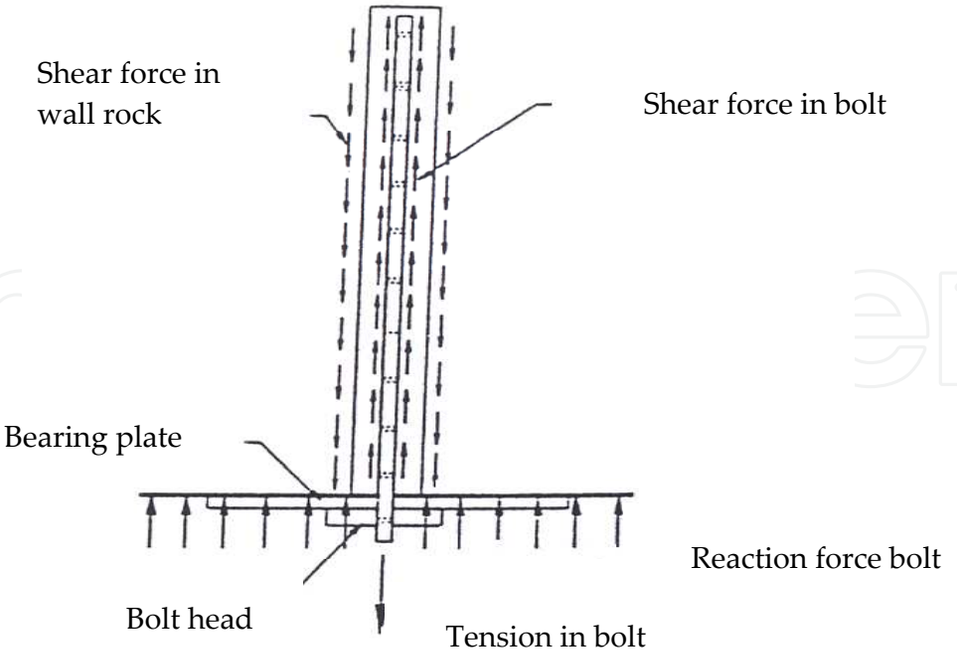

Figure 3. Bolt-Rock interaction model (after Peng and Guo, 1992)

Stankus and Guo (1996) investigated that in bedded and laminated strata, point anchor and fully grouted bolts are very effective, especially if quickly installed at high tension after excavation. They used three lengths 3300, 2400, and 1500 mm and three tensions, 66, 89, and 110 kN and found that:

- Bolts with higher pre-tension induce a smaller deflection
- The longer the bolt, the larger the load,
- In bolts with the same length and high tension, there is small deflection,
- Large beam deflection was observed in long bolts and small deflection in short bolts.

They developed a method for achieving the optimum beaming effect (OBE). However there were some assumptions in their methodology such as, the problem with the gap element, which is not flexible for any kind of mesh, especially with thin grout. Many relevant parameters about the contact interface cannot be defined in gap element. All materials were modelled in the elastic region.

Marence and Swoboda (1995) developed the Bolt Crossing Joint (BCJ) element that connects the elements on both sides of the shear joint. It has two nodes, one each side of the discontinuity. The model cannot predict the de-bonding length along the bolt, grout interface and hinge point position.

It was realised that to further facilitate data analysis and the stress and strain build up along a bolt surrounded by composite material and their interaction, a powerful computer simulation was needed. FE modelling is considered to be the only tool able to accomplish this goal. There is still a lack of an adequate global models of grouted bolts to analyse bolt behaviour properly, particularly at the contact interfaces.

In this chapter, three-dimensional formulations and non-linear deformation of rock, grout, bolt, and two interfaces are taken into account in the reinforced system. A description of the numerical model developed is presented below.

4. Materials design model

The FE method is the most suitable computational method to evaluate the real behaviour of the bolt, grout, and surrounding rock when there are composite materials with different interfaces. A three dimensional FE model of a reinforced structure subjected to shear loading was used to examine the behaviour of bolted rock joints. Three governing materials (steel, grout, and concrete) with two interfaces (bolt-grout and grout-concrete) were considered. To create the best possible mesh, symmetry rules should be applied. To reduce computing demand and time (when a fine mesh is used) the density of the mesh has been optimised during meshing. The division of zones into elements was such that the smallest elements were used where details of stress and displacement were required. The process of FE analysis is shown in Figure 4.

4.1. Modelling concrete and grout

Care was taken to develop the best model for concrete and grout that could offer appropriate behaviour. 3D solid elements, Solid 65 that has 8 nodes was used with each node having three translation degrees of freedom that tolerates irregular shapes without a significant loss in accuracy. Solid 65 is used for the 3-D modeling of solids with or without reinforcing bars (rebar). The geometry and node locations for this type of element are shown in Figure 5 a. The solid element is capable of plastic deformation, cracking in tension, crushing in compression, creep non-linearity, and large deflection geometrical non-linearity, and also includes the failure criteria of concrete Fanning (2001), Feng et al. (2002) and Ansys (2012). Concrete can fail by cracking when the tensile stress exceeds the tensile strength, or by crushing when the compressive stress exceeds the compressive strength. A FE mesh for concrete is shown in Figure 5 b. Figure 6 shows the FE mesh for grout. Due to symmetry only a quarter of the model needed to be treated.

4.2. Modelling the bolt

The steel bar, which resists axial and shear loads during loading, due to rock movement, is the main element within the rock bolt system,. The steel bar was modelled appropriately, particularly with regard to the type of element designed and bolt behaviour, in the linear and non-linear region. 3D solid elements, solid 95 with 20 nodes, was used to model the steel bar, with each node having three translation degree of freedom. The approach adopted is to reveal that the experimentally verified shear resistance of fully grouted bolt can be investigated by numerical design. Elastic behaviour of the elements was defined by Young's Modulus and Poisson's ratio of various materials. The stress, strain relationship of steel is assumed as the bi-linear kinematic hardening model and the modulus of elasticity of strain hardening after yielding, is accounted as a hundredth of the original one, *Cha et al.* (2003),

Hong et al. (2003) and *Abedi et al*. (2003). Figure 7 displays the solid 95 elements and FE mesh for bolt.

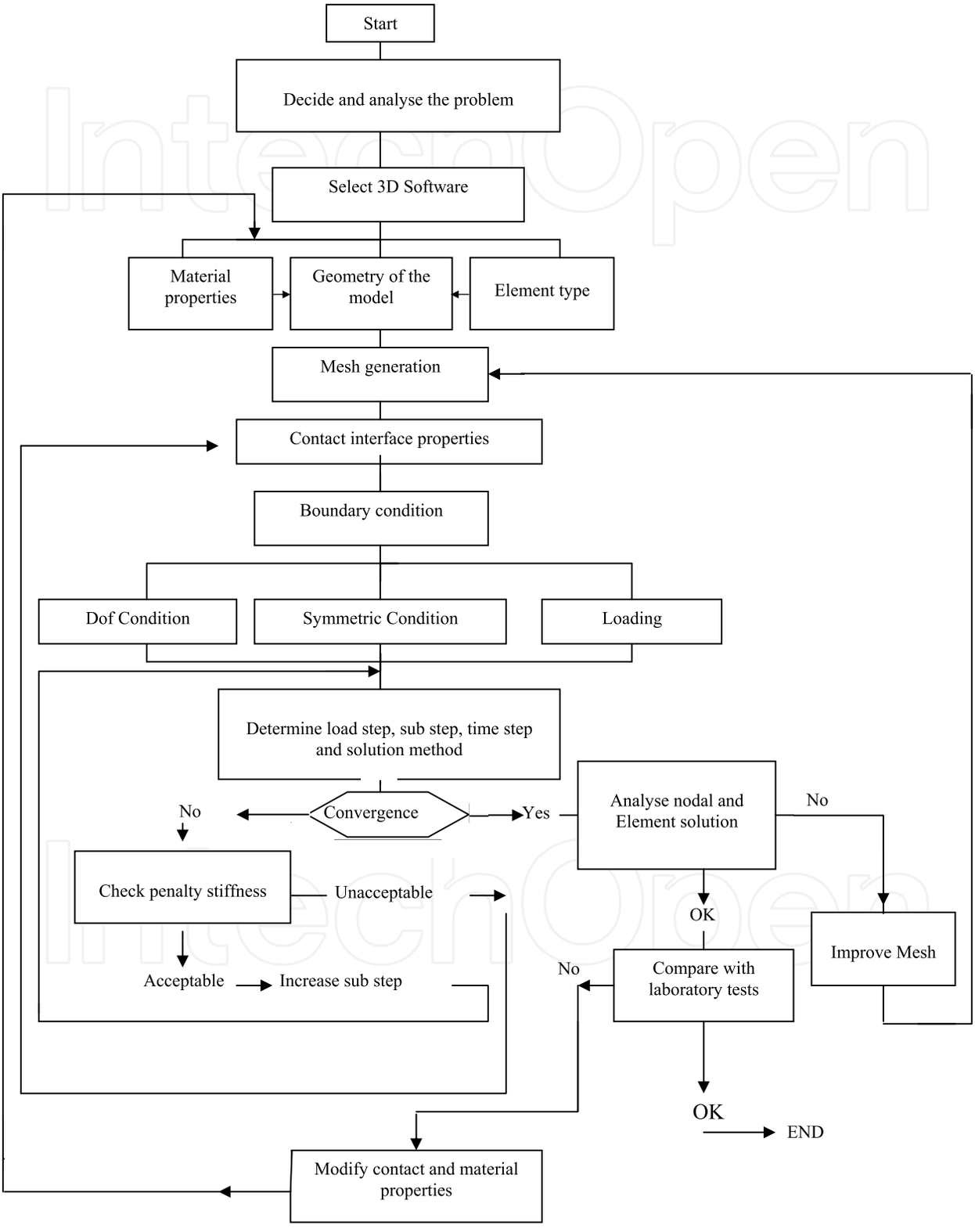

Figure 4. The process of FE simulation (Dof = degrees of freedom)

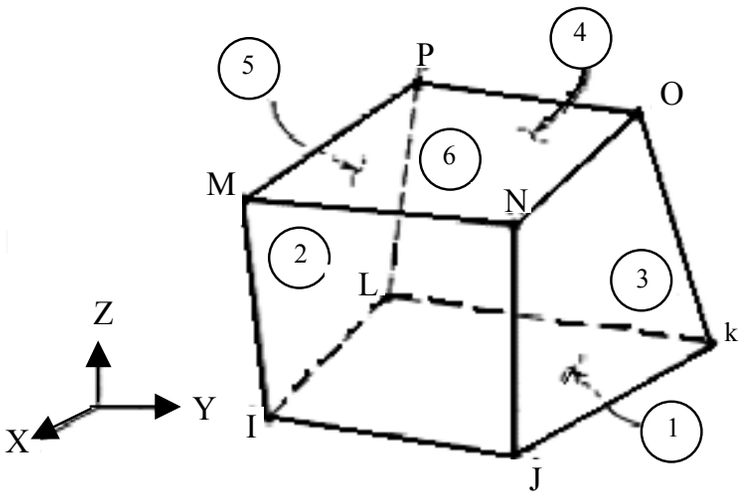

(a)

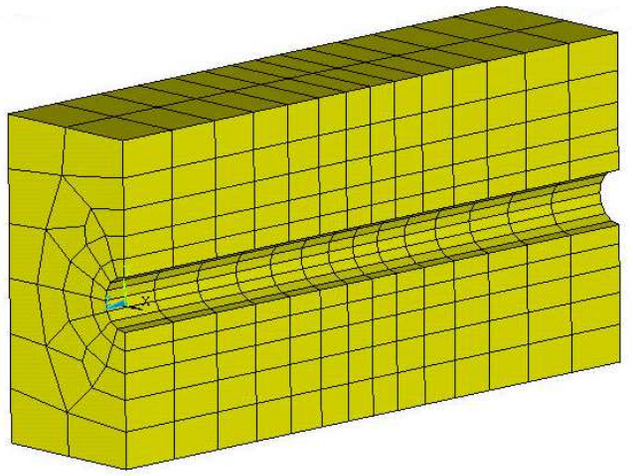

(b)

Figure 5. (a) 3D Solid 65 elements; (b) Concrete mesh

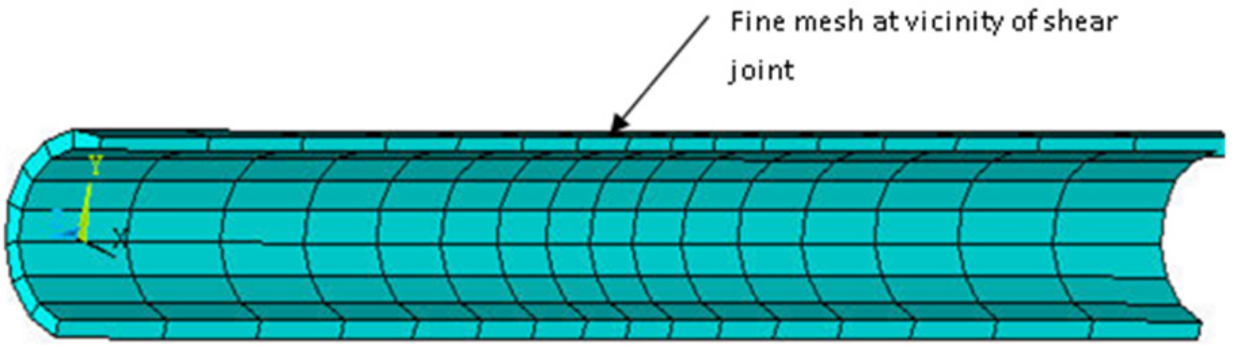

Figure 6. FE mesh for grout

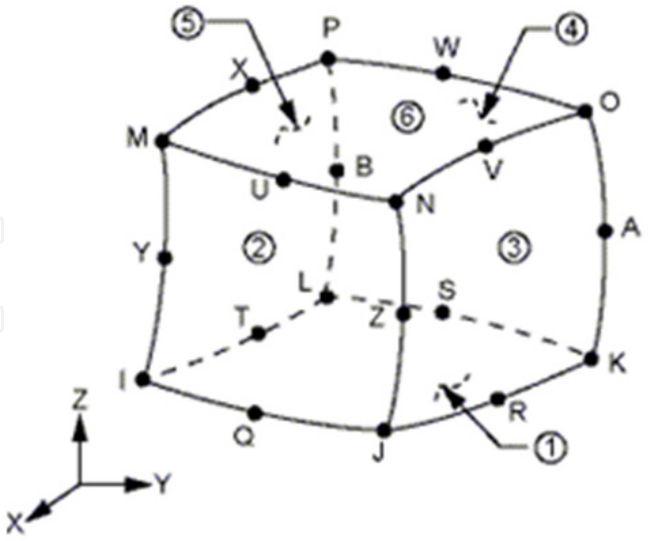

(a)

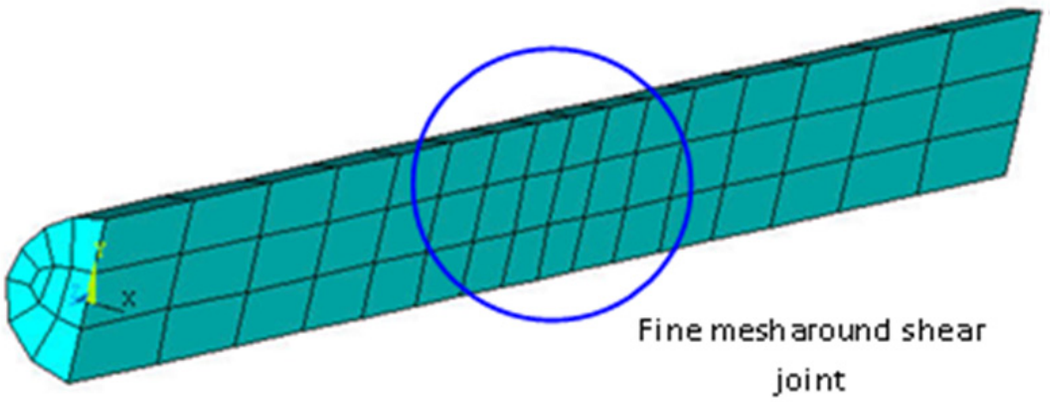

(b)

Figure 7. (a) 3D Solid 95 elements (b) FE mesh for bolt

4.3. Contact interface model

The main difficulties with numerically simulating a reinforced shear joint are the bolt- grout and grout-rock interfaces. An important parameter controlling the load transfer from the bolt to the rock through resin is bond behaviour between the interfaces. If they are not designed properly it is difficult to understand their behaviour, when and where de-bonding occurs, how a gap is created between the interfaces, and how the load is transferred. Thus the contact interfaces were designed to act realistically. To study the stress, strain generation through numerical modelling, it is very important to model the interfaces accurately, *Pal et al.* (1999). *Ostreberge* (1973) also emphasised the bond strength between two adjacent

mediums for an accurate load transfer. *Nietzsche and Hass* (1976) proposed a model for bolt, grout-rock that assumed a linear elastic behaviour for all materials, and perfect bonding for all contact interfaces (bolt- grout and grout- rock). It has to be noted that perfect bonding, particularly between the bolt-grout interface could not be considered to be the right behaviour, because there is no cohesion strong enough between them. In addition, there are large stresses and strains concentrated near the shear joints, which restrict perfect bonding. The interface between the grout and concrete was considered as standard behaviour where normal pressure changes to zero when separation occurs. As found from laboratory results, a low cohesion (150 kPa) was adopted for the contact interface, which was determined from the test results under constant normal conditions.

3D surface-to-surface contact element (contact 174) was used to represent contact between the target surfaces (steel-grout and rock - grout). This element is applicable to 3D structural contact analysis and is located on the surfaces of 3D solid elements with mid-side nodes. This contact element is used to represent contact and sliding between 3-D "target" surfaces (Target 170) and a deformable surface, is defined by this element. The element is applicable to three-dimensional structural and coupled thermal structural contact analysis. This element is also located on the surfaces of 3-D solid or shell elements with mid-side nodes. It has the same geometric characteristics as the solid or shell element face to which it is connected. Contact occurs when the element surface penetrates one of the target segment elements on a specified target surface. The contact elements themselves overlay the solid elements describing the boundary of a deformable body and are potentially in contact with the target surface. This target surface is discritised by a set of target segment elements (Target 170) and is paired with its associated contact surface via a shared real constant set. Figure 8 displays the target 170 geometry.

4.4. 3D geometrical model

An actual 3D geometrical model was created to simulate the rock-bolt- grout behaviour and their interactions. The model bolt core diameter (D_b) of 22 mm and the grouted cylinder (D_h) of 27 mm diameter had the same dimensions as those used in the laboratory test. Due to the symmetry of the problem, only one fourth of the system was considered. Figure 9 shows the geometry of the FE model with mesh generation.

5. Verification of the model

A numerical representation model for a fully grouted reinforcement bolt was developed and its validity assessed with laboratory data conducted in a variety of rock strengths and pre-tension loadings. A comparison of experimental results with numerical simulations showed that the model can predict the interaction between bolt, grout, and concrete, and how the interfaces behave. The consistency of the experimental observations with a numerically design model is presented by typical shear load, shear displacement curves shown in Figure 10. It is clear that when the strength of the concrete was doubled there was a twofold reduction in shear displacement.

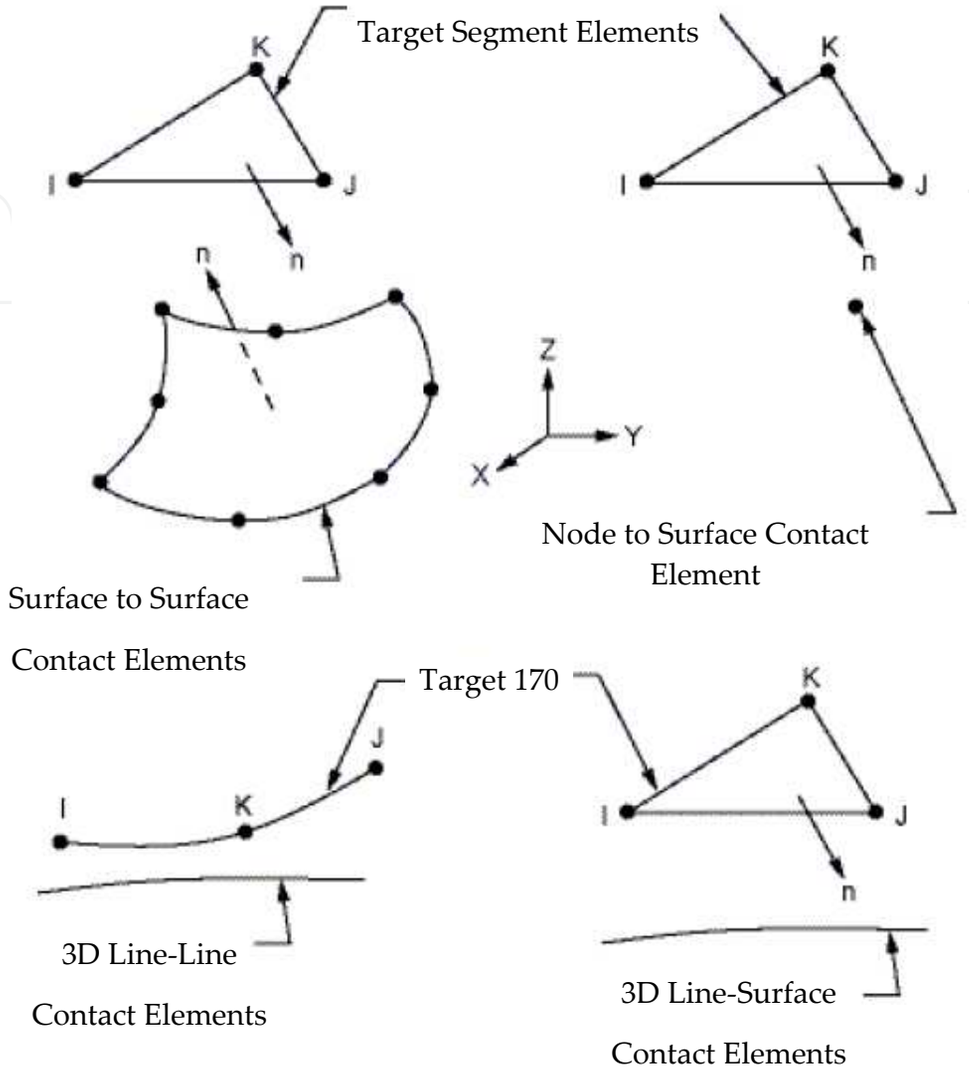

Figure 8. Target 170 geometry (Ansys 2012)

6. Modelling bolts under lateral loading

An extensive series of laboratory tests to analyse the bending behaviour of fully grouted bolts in different strength rock, bolt pre-tension and thickness of resin were carried out. Three governing materials (steel, grout, and rock) with two interfaces (bolt-grout and grout-rock) were considered for 3D numerical simulation.

By this three dimensional FEM, the characteristics of elasto - plastic materials and contact interfaces are simulated. Numerical modelling in different strength rock (20, 40, 50 and 80 MPa) and different pre-tension loads (0, 20, 50, and 80 kN) were carried out and the results were analysed. As the output results were large, only the main results of 0 and 80 kN pre-tension are presented here.

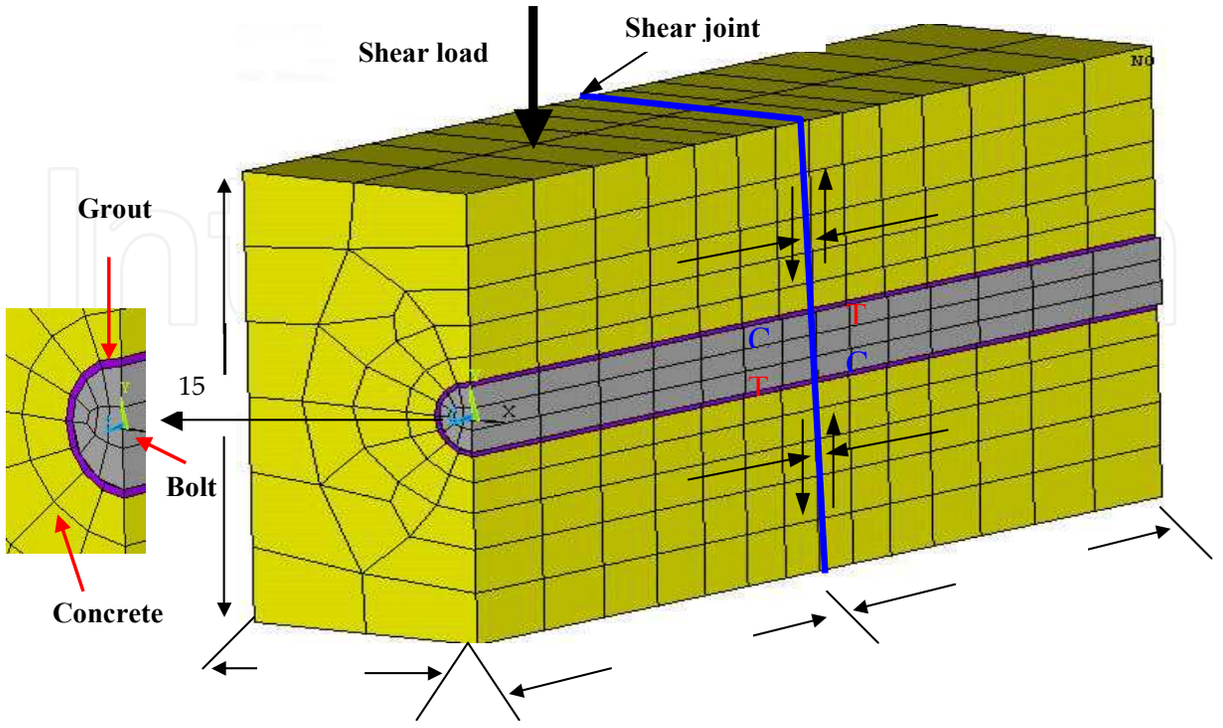

Figure 9. Geometry of the model and mesh generation

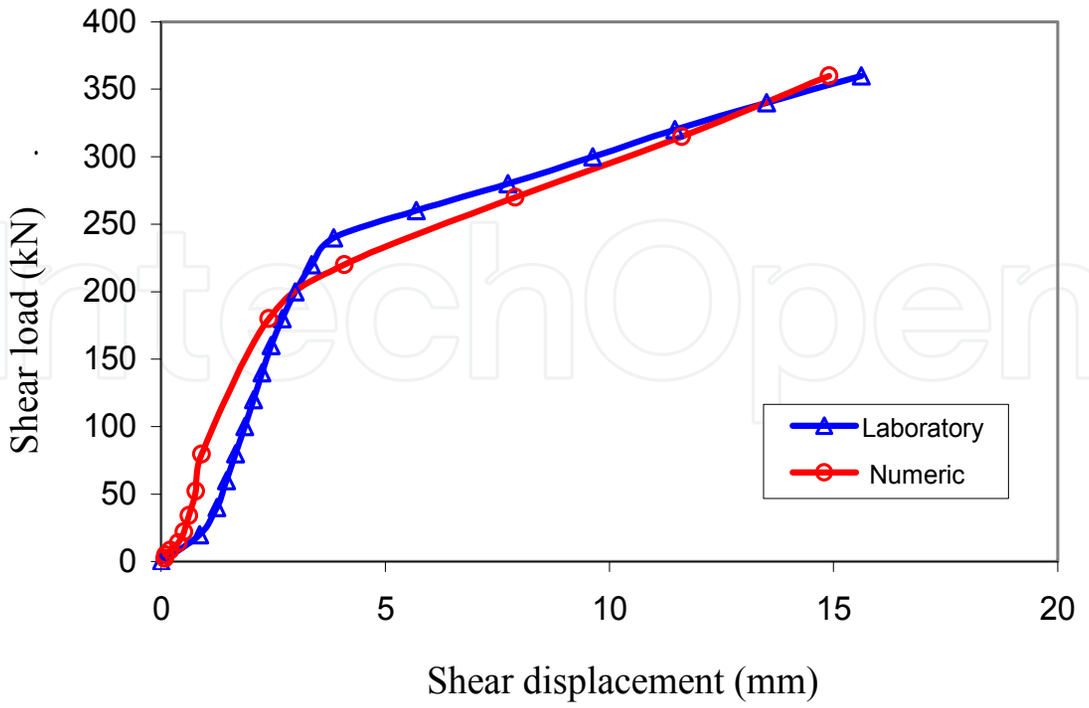

Figure 10. Load-deflection in 80 kN pretension bolt load and 40 MPa concrete

6.1. Bolt behaviour

6.1.1. Stresses developed along the bolt

When a beam with a straight longitudinal axis is loaded laterally, its longitudinal axis is deformed into a curve, and the resulting stresses and strains are directly related to the deflection curve, which is affected by the surrounding materials. Figure 11 shows a quarter of the model with induced loads along the shear joint.

When the beam was bent there was deflection and rotation at each point. The angle of rotation α is the angle between the bolt axis and the tangent to the deflection curve, shown as point o. α was measured for the bolts tested. The deflection trend in 20 MPa concrete is shown in Figure 12.

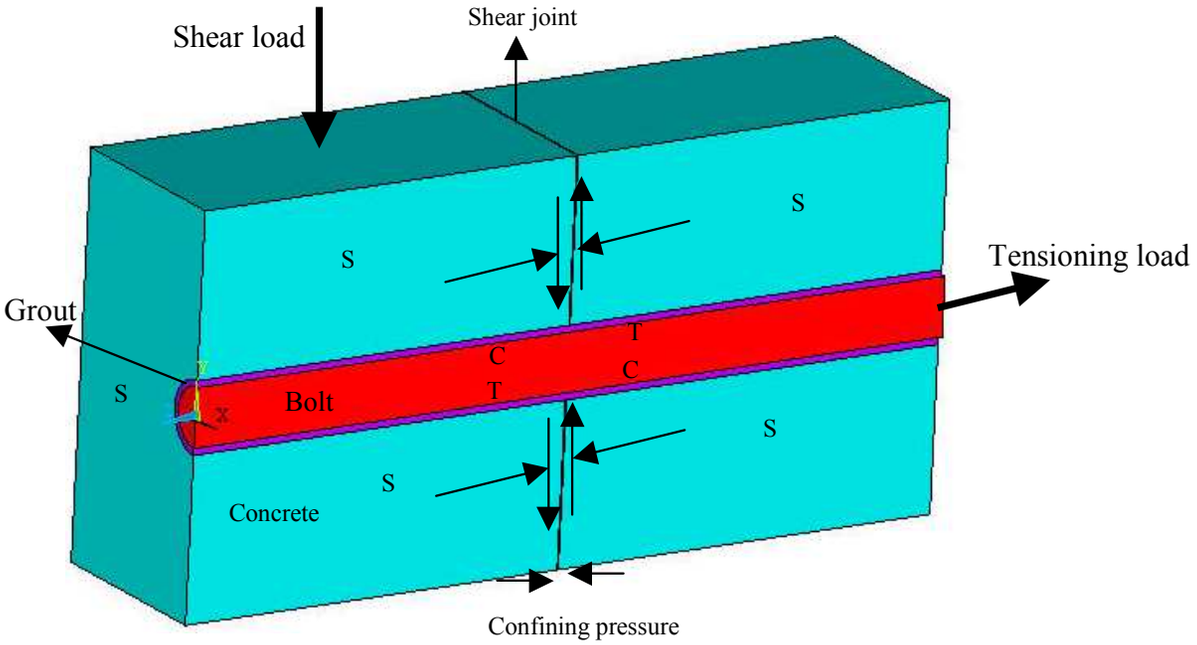

Figure 11. Numerical model (s = symmetric planes, c = compression zone, T = tension zone

Also to find the relationship between deflection and each point along the axis of the bolt, raw output data from the numerical simulation were classified and entered as input data to Maple software. Equation 3 and Figure 13 were established.

$$\tan\alpha = \frac{dv}{dx}, \tag{1}$$

$$\alpha = \arctan\frac{dv}{dx} \tag{2}$$

$$U_y = -40.76 + 26\,Arc\tan(e^{(0.05x-7.2)}) \tag{3}$$

where;

- U_y = Shear displacement (mm)
- x = Distance from the bolt centre to the end (mm), from A to B.

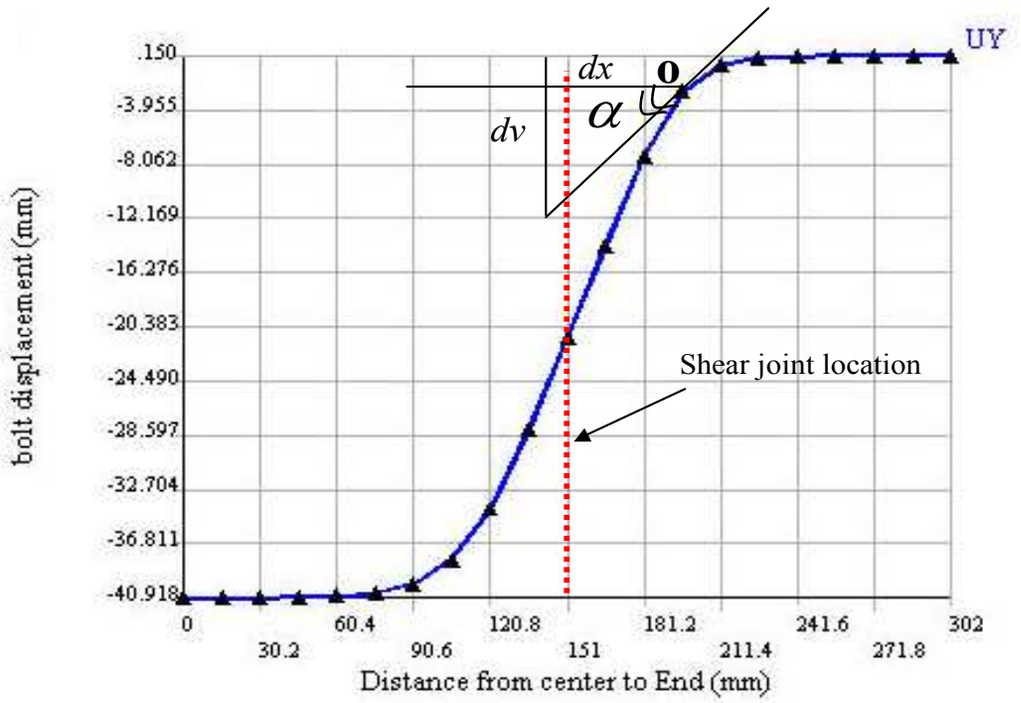

Figure 12. Bolt displacement in 20 MPa, without Pre-tension

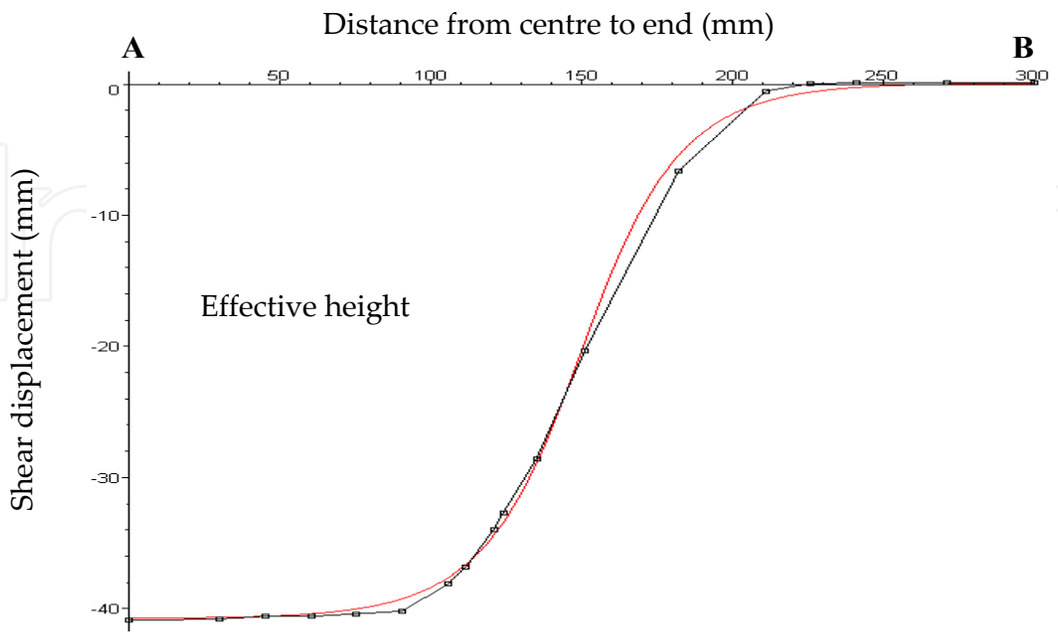

Figure 13. Shear displacement as a function of bolt length sections in 20 MPa concrete

The relationship between vertical displacement at the bolt-joint intersection and hinge point is:

$$Uy\ (hinge) = (0.15\text{-}0.2)\ Uy\ (joint)$$

Which is consistent with the laboratory results. Figure 14 shows the bolt deflection in 40 MPa concrete.

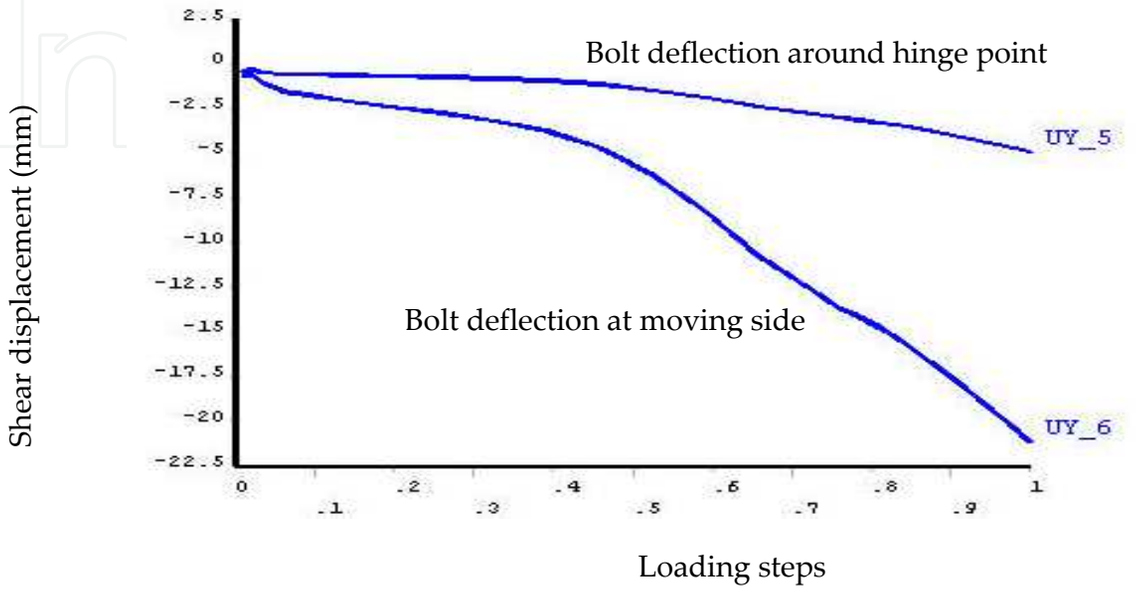

Figure 14. Bolt deflection at the moving side and hinge point versus loading process, in 40 MPa concrete without pre-tension load

Figure 15 shows the contours of stress developed along the bolt in 20 MPa concrete, where the stress in the top part of the bolt and towards the perimeter are tensile and compressive at the centre. However, the stress conditions at the lower half section of the bolt are reversed. In addition, the shape of the bolt between the hinges can be considered as linear. The rate of stress changes in the post failure region is plotted in Figure 16.

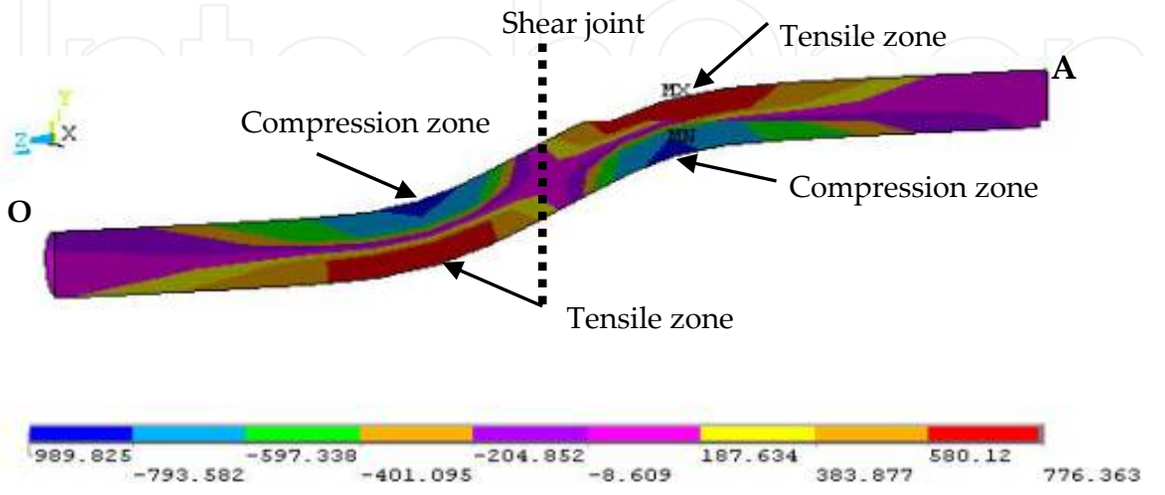

Figure 15. Stress built up along the bolt axis in 20 MPa concrete without pre-tension

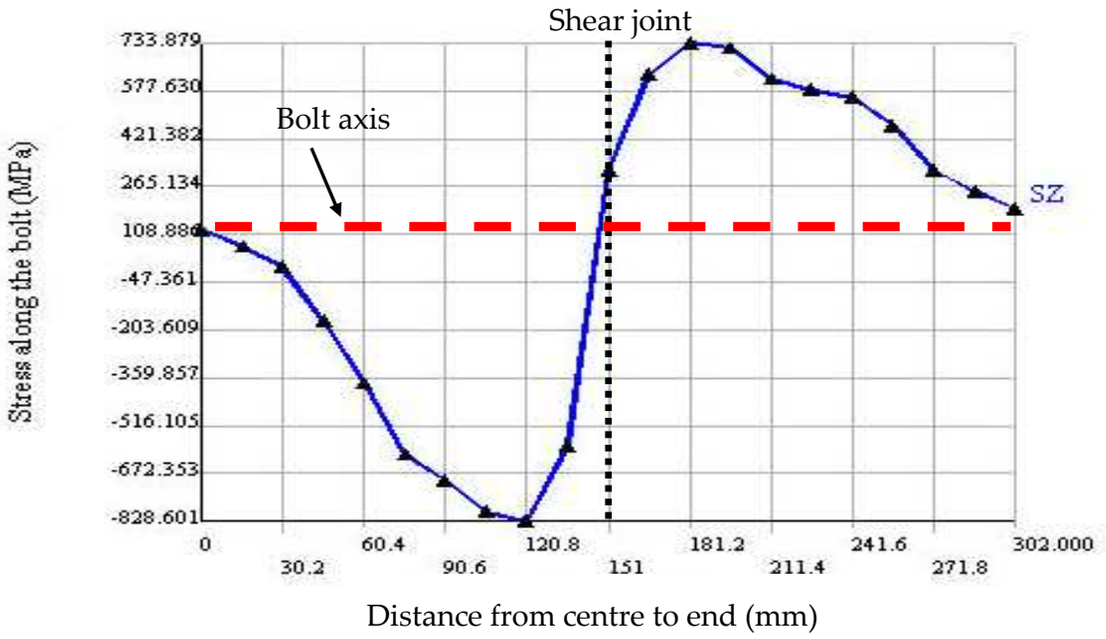

Figure 16. Trend of stress built up along the bolt axis 20 MPa concrete with 80 kN pre-tension

It can be seen that induced stresses at these tensile and compression zones are high and the bolt appears to be in a state of yield. At the two hinges the yield limit of the bolt is reached quickly. However, a further increase in the shear load has no apparent influence on the stress built up at the hinge point. From this stage afterwards, only tensile stresses are developed and expanded between the hinge points, and may lead the bolt to fail at some distance between the hinge points located near the shear joint, as the maximum stress and strain occurs between them.

From analysing the results in different pre-tension loads it was found there are no significant changes in induced stresses along the bolt with an increase in pre-tension load in the tension zone. However there is a slight reduction in compressive stress with an increasing pre-tension load. Induced stresses are higher than the yield point and less than the maximum tensile strength of the steel bolt in both situations (with and without pre-tension in all strength concrete). Moreover, in different strength concrete it was observed that the strength of the concrete affects shear displacement and bolt contribution. However there were no meaningful changes in induced stress beyond the yield point along the bolt axis with increasing rock strength but stress was reduced slightly with high pre-tension loading and strength of concrete. The Von Mises stress trend along the bolt axis perpendicular to the shear joint in 20 MPa concrete is plotted in Figure 17. Comparing the results in 20 MPa concrete with and without pre-tension, Von Mises stress decreased slightly, with an increase in bolt pre-tension. However, this difference is insignificant.

Figure 18 shows the concentration of shear stress along the bolt and the rate of change along the axis is shown in Figure 19. Figure 20 shows the trend of shear stress along the length of the bolt in one side of the joint surrounded with soft concrete.

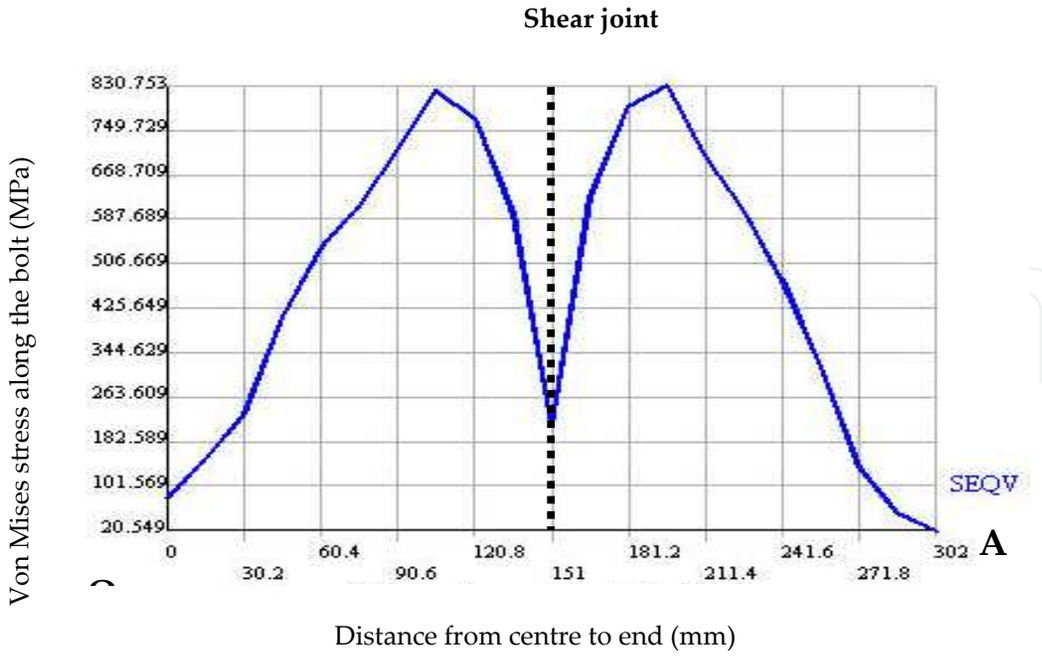

Figure 17. Von Mises stress trend in 20 MPa concrete without pre-tension

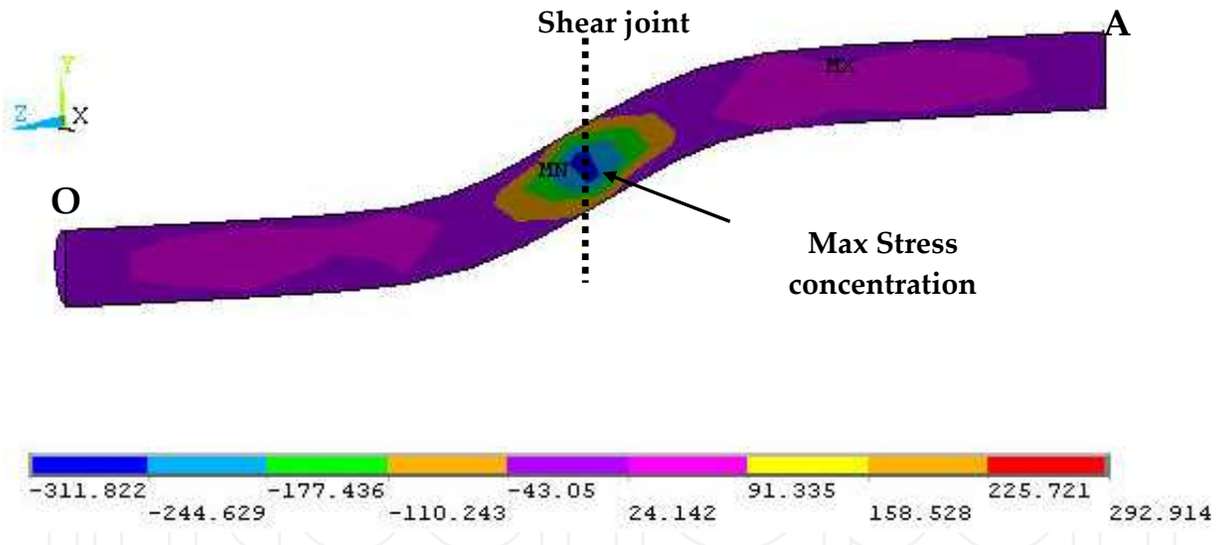

Figure 18. Shear stress contour in the concrete 20 MPa without pre-tension

As it shows the maximum shear stress is concentrated in the vicinity of the joint plane, and according to structural analysis, the bending moment at this point is zero. These stress slowly increase, beginning with plastic deformation, and end with a stable situation. The shear stress reduces dramatically from the shear joint towards the bolt end. This trend reaches zero at the hinge point. In the two hinges, the yield limit of the steel is reached quickly, at about 0.3 P and 0.4 P in concrete 20 and 40 MPa respectively, (P is the maximum given applied load). Further increase in the shear force has no apparent influence on stress in the hinges. The distance between the hinge points is reduced as the strength of the concrete is increased.

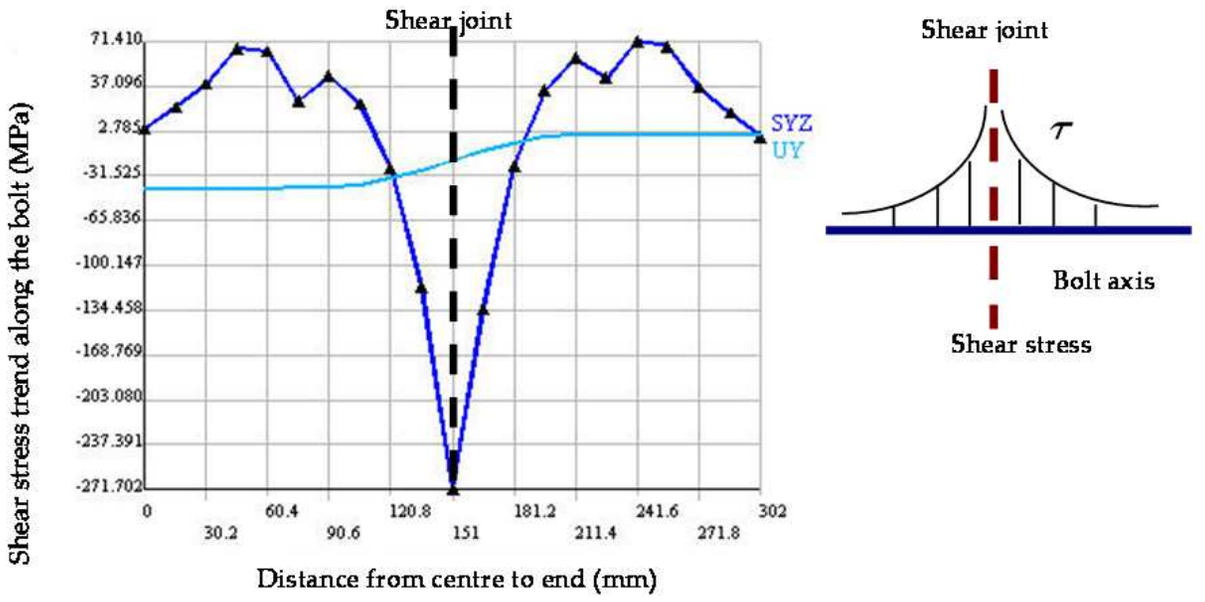

Figure 19. The rate of shear stress change along the bolt axis in concrete 20 MPa without pre-tension

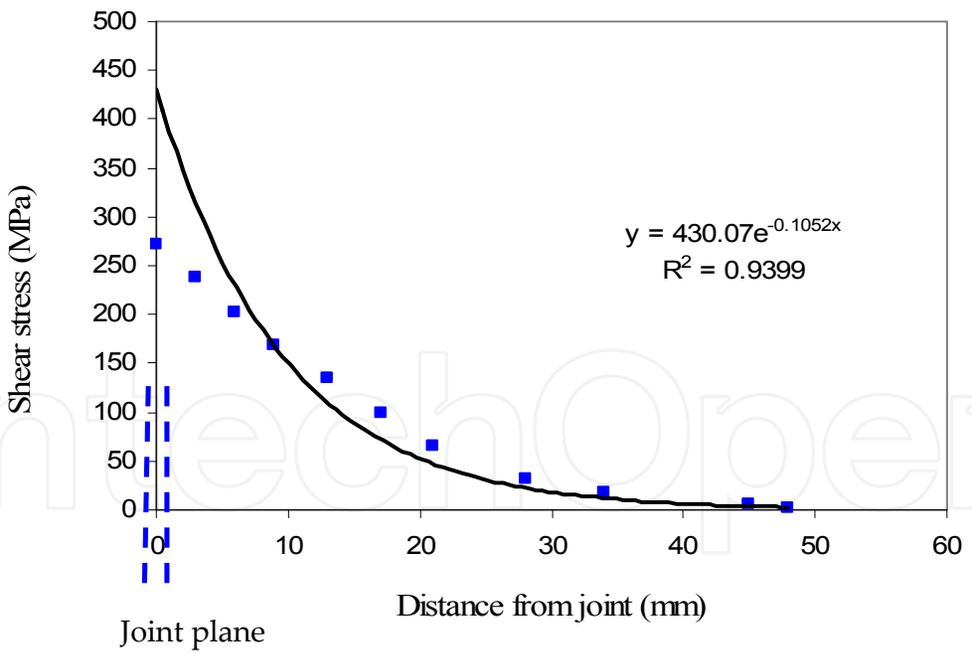

Figure 20. The rate of shear stress along the bolt axis in concrete 20 MPa without pre-tension in one side of the joint plane

Figure 21 shows the trend of changes in shear stress profile with the shear stress tapering off to a stable state past the yield point. It shows the shear stress trend is not exceeded during further loading after the yield point.

Eventually, a combination of this stress with induced tensile stress at the bolt - joint intersection leads the bolt to fail. By increasing the initial tensile load on the bolt, the shear stress was decreased, which was seen in different strength concrete but there was no significant changes with increasing shear load after the yield point. Any reduction in shear stress causes an increase in the resistance of the bolt to shear. It can be noted that the shear stress increased slightly with an increasing strength of concrete.

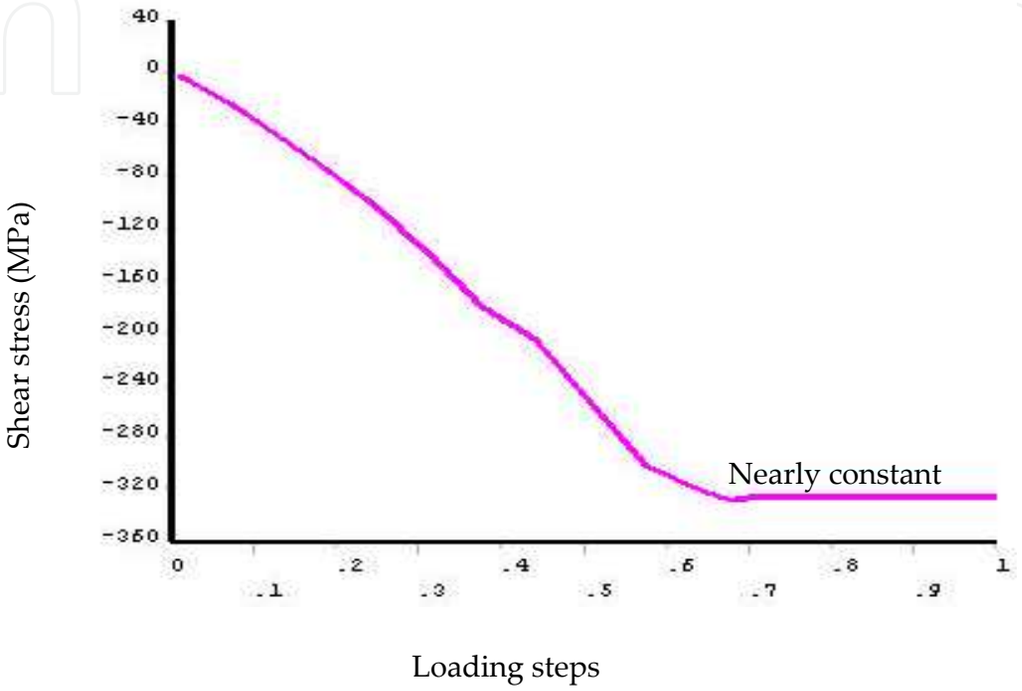

Figure 21. Shear stress trend in bolt –joint intersection in concrete 20 MPa at post failure region without pre-tension load

6.1.2. Strain developed along the bolt

Strain was generated along all the surrounding materials as the shear load increased, particularly along the axis of the bolt. As deflection increased, plastic strain is induced in the critical locations in all three materials (bolt - resin and concrete). Figure 22 shows the location of maximum plastic deformation along the bolt while bending. It shows there are two hinge points around the shear plane approximately 50 mm from the shear joint in 20 MPa concrete.

However an increasing pre-tension load has not affected hinge point distances, which are around 2.3 D_b (D_b is bolt diameter). This value in the laboratory test is around 44 mm that is 2 D_b. The strain and the rate of strain changes along the bolt in 20 MPa concrete are shown in Figures 23 and 24.

As Figure 23 shows that the outer layer of the bolt yielded, whereas the middle section remained in an elastic state.

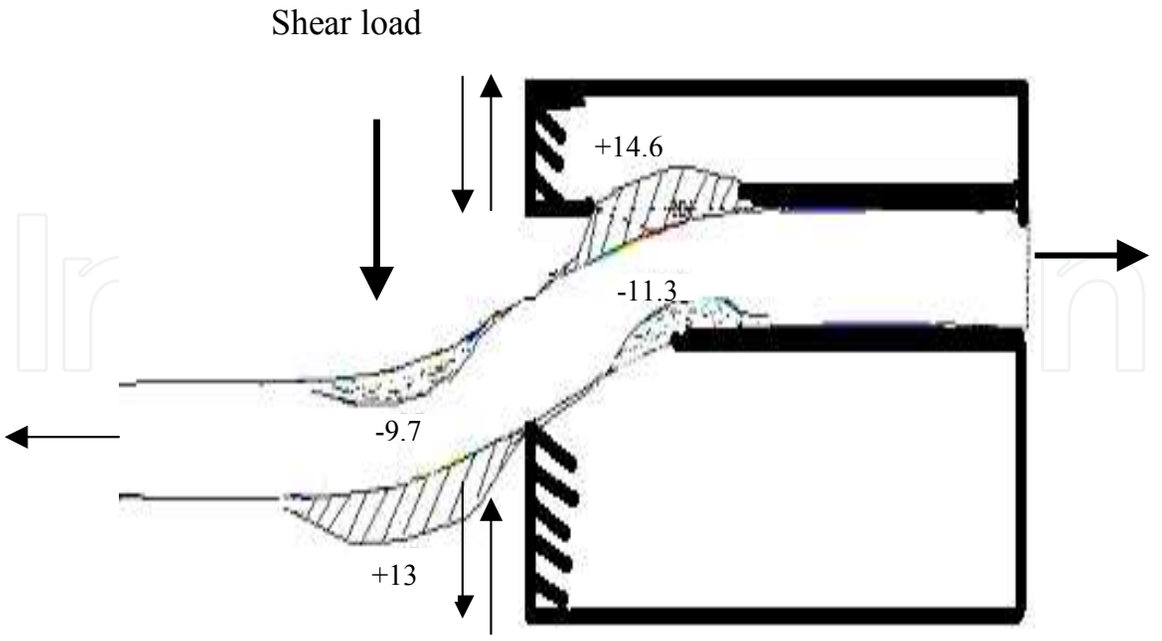

Figure 22. Deformed bolt shape in post failure region in 20 MPa concrete

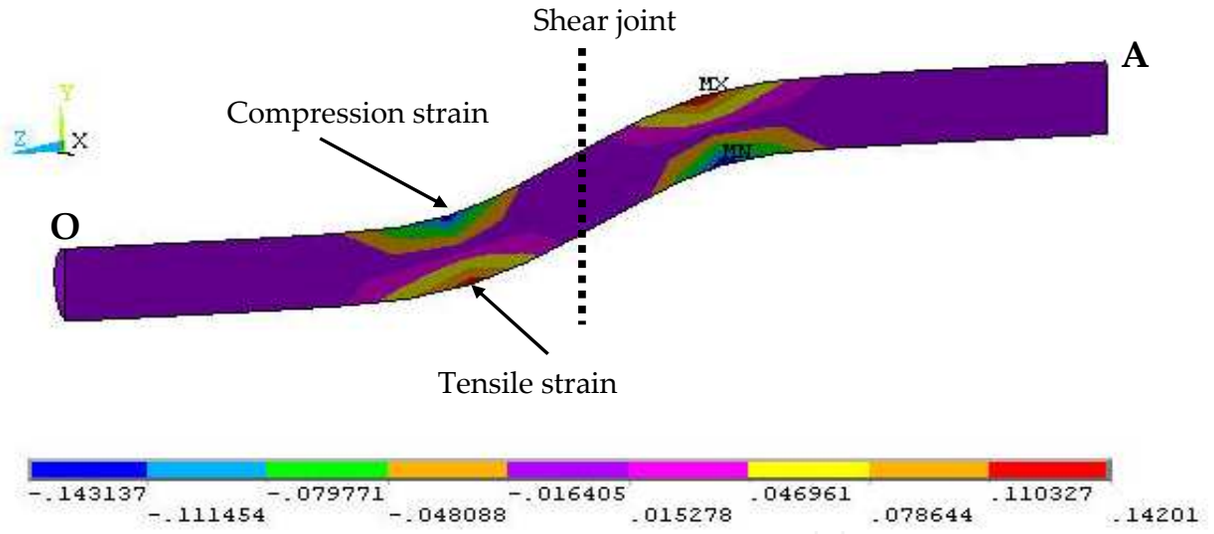

Figure 23. Plastic strain contour along the bolt axis in concrete 20 MPa without pre-tension

Figure 25 shows the beginning of plastic strain during shearing and a trend of strain developing as a function of load stepping. It notes that both the tensile and compression strain around the bolt started approximately 27-30 % after loading began and increased with an increasing shearing load. However, the rate of increase in the tensile zone is higher than the compression zone. It also showed these strains appeared in the early stage of loading with a small displacement (around 3 mm), which increased with increase in shear deflection.

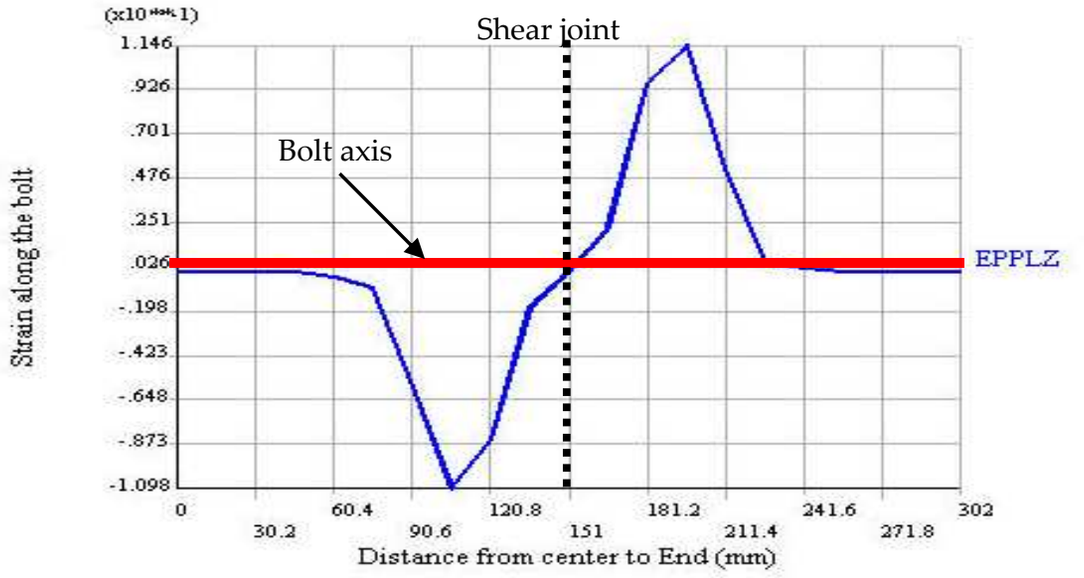

Figure 24. Strain trend along the bolt axis in concrete 20 MPa without pre-tension in upper fibre of the bolt

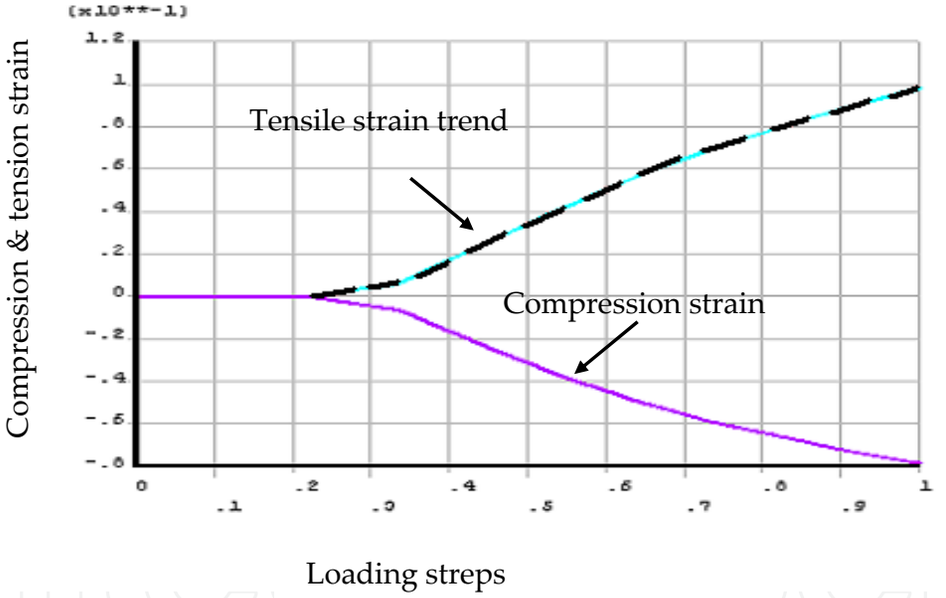

Figure 25. Yield strain trend as a function of time stepping concrete 20 MPa in 20 kN pre-tension load

With an increase in loading, shear displacement was increased. There was a significant increase in shear displacement after 35% of loading time. Bending of the bolt is predominant at a low loading time. plastic strain begins at the hinge point around 35 % of loading. A comparison of the data (with and without pre-tension) shows that the intensity of the strain along the axis of the bolt is slightly reduced with an increase in pre-tension load. However the affected area in the tensile zone expands towards the shear joint. The strains in the compression and tension zones were reduced in higher strength concrete.

6.2. Concrete behaviour

6.2.1. Stress developed in concrete

The behaviour of the centre concrete under shear load in double shearing assembly was analysed in different strength concrete and different pre-tension loads. During shearing the middle part of the assembled system was displaced downwards with increasing shear load. Figure 26 shows the deflection rate after failure. Reaction forces are developed during the middle concrete block displacement, which increased in critical locations (at the vicinity of the shear joint), affected by the bolt. The reaction forces induce and propagate stress and strain in sheared zones. Figure 27 shows the high-induced stress near the shear joint as the maximum reaction forces are expected there. When induced stress is larger than the ultimate stress the concrete will be crushed. Figure 28 displays the rate of induced stress at the interface near the shear joint. It shows that induced stresses are much higher than the compressive strength, and the concrete at this location would be severely crushed. From the figure it can be seen that the high stress is approximately 60 mm from the shear plane. At an early stage of loading, the concrete was crushed and stresses propagated throughout, with bolt yield to start at around 2 mm from the edge of the intersection. Beyond this point stresses increased quickly near the joint intersection and reaction zones. Induced stresses near the shear joints were reduced slightly with increase in the pre-tension load on the bolt. In addition the trend of induced stresses and strains built up along the concrete interface in 40 MPa concrete was the same as with 20 MPa concrete. However, the value of stresses and strains were slightly reduced in higher strength concrete.

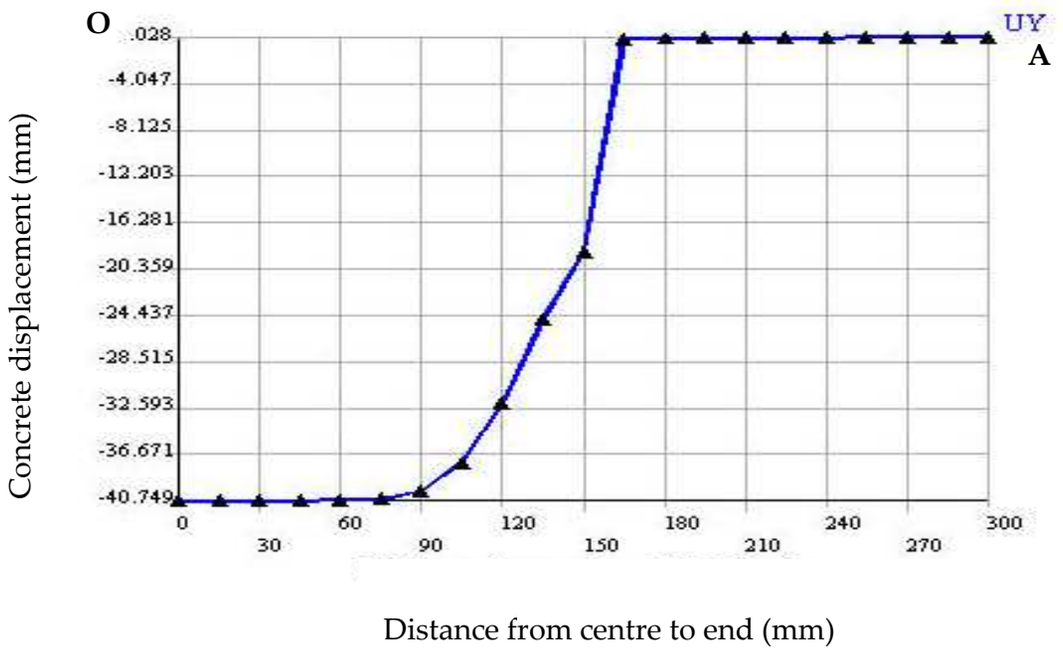

Figure 26. Concrete displacement in non-pretension condition in 20 MPa concrete

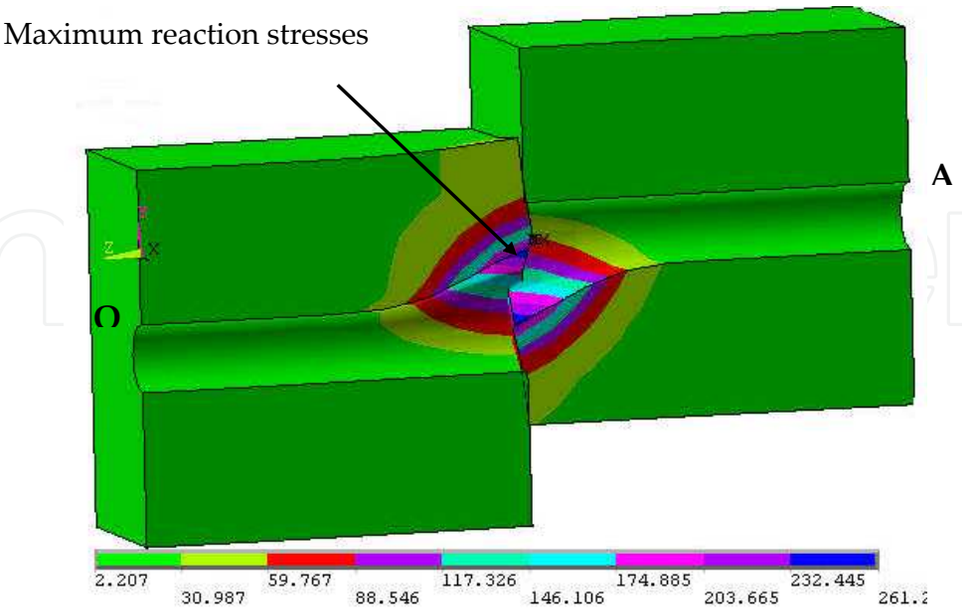

Figure 27. Yield stress induced in 20 MPa concrete without pre-tension condition

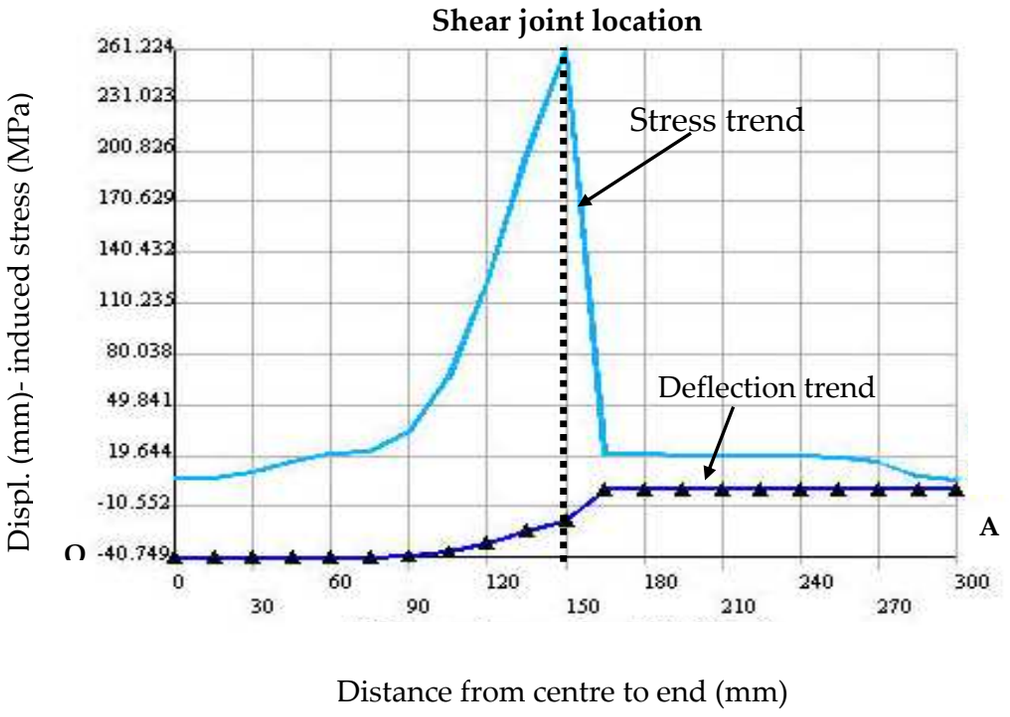

Figure 28. Induced stress and displacement trend in 20 MPa concrete without pre-tension

6.2.2. Strain developed in concrete

The highest level of induced stress was near the shear joint, so it is expected that strain would be highest around this zone. Figure 29 shows the induced strain contours at the high pressure zone. Figure 30 shows induced strain in terms of loading time in grout and concrete. It shows that the strain generation begins in the concrete before it is seen in the resin grout because lower strength concrete is one third the strength of grout. There is an approximate exponential relationship in the strain trend as loading increases. After 20% of loading steps, plastic strain is induced along the contact interface near the shear joint. This value in soft concrete (20 MPa) is at an earlier stage, which is around 15% of loading step. This shows the strain built up along the axis of the bolt is lower than in the shear direction.

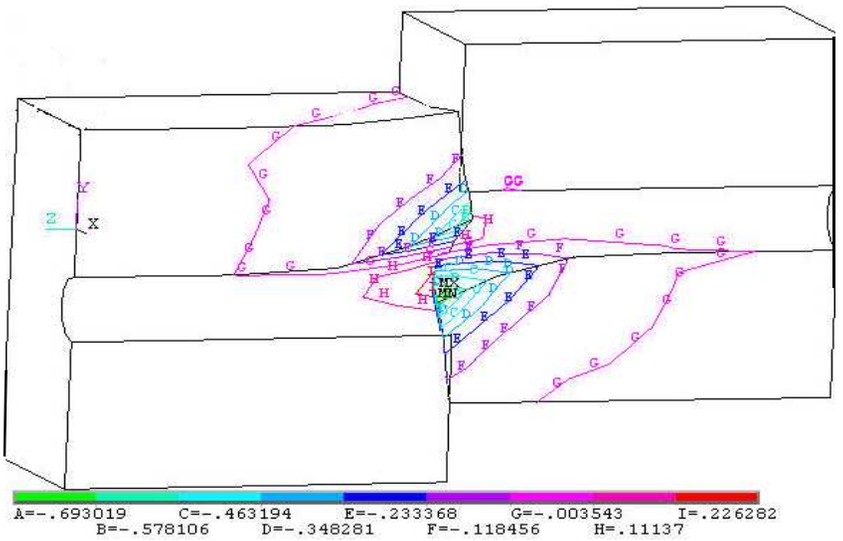

Figure 29. Strain contours in 20 MPa concrete without pre-tension

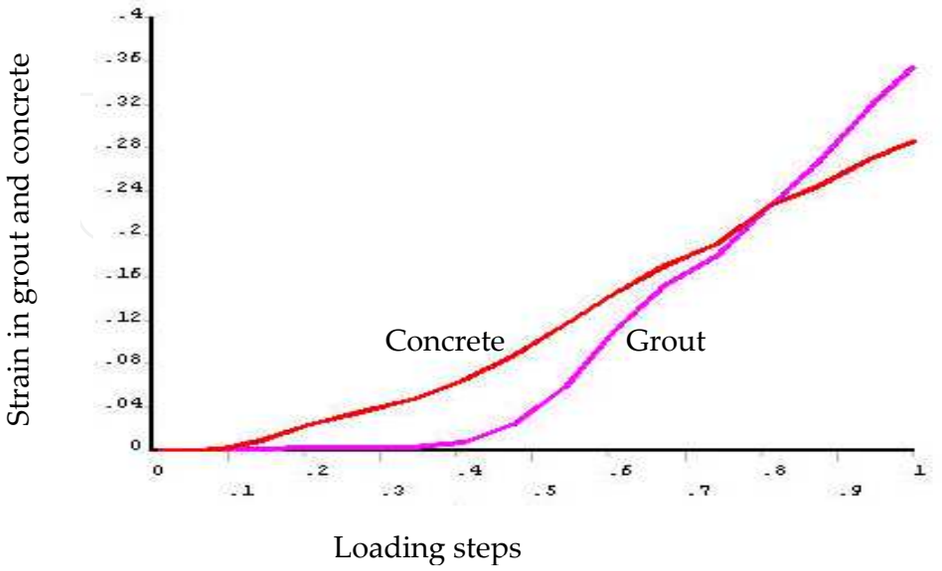

Figure 30. Induced strain in concrete 20 MPa in grout and concrete versus loading without a pre-tension and 27 mm diameter hole

A comparison of induced strain along the joint interface with and without pre-tension found that the strain in the shear direction is reduced (around 15%) with increasing pre-tension. In the axial and shear direction strain was concentrated near the shear joint.

Figure 31 shows the deformation behaviour of both concrete medium and bolt. Plastic deformation of concrete occurs nearly 15 % of the maximum shear load while the deformation of the bolt occurs at 33% of the loading steps. From the graphs it can be inferred that in very low values of bolt deflection and time steps, fractures happen in the concrete, which is in the elastic range of the bolt. Any further increase in shearing does not influence the stress at the hinge points, however induced stress in the concrete blocks causes extensively fractures and eventually leads to failure.

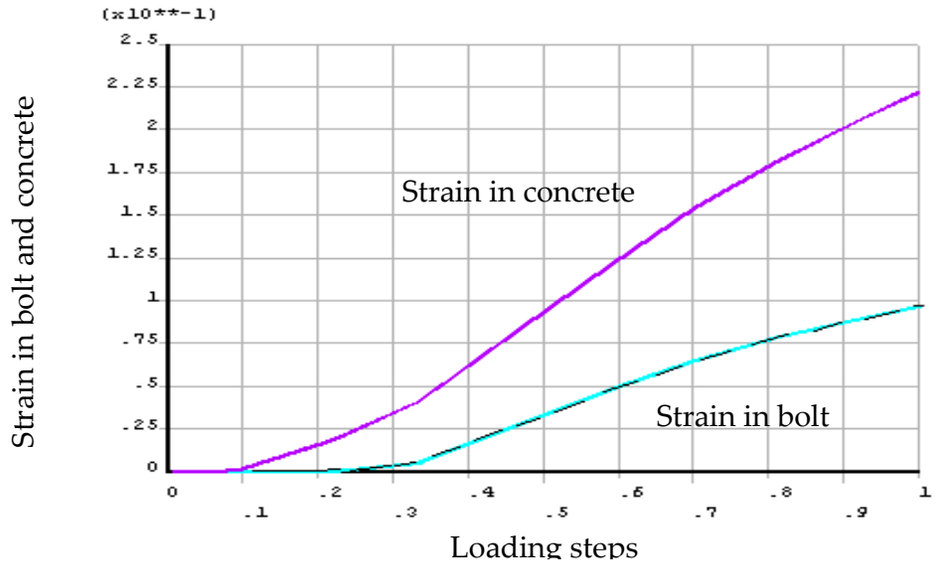

Figure 31. Induced strain in concrete and bolt as a function of loading steps in 20 MPa concrete with 80 kN pre-tension

6.3. Grout behaviour

6.3.1. Stress in grout

It is known that grout bonds the shanks to the ground making the bolt an integral part of the rock mass itself. Its efficiency depends on the shear strength of the bolt - grout, and grout - rock interface. Figure 32 shows the contours of induced stress through the resin layer surrounded by 20 MPa concrete, without pre-tension. It was revealed that the induced stress exceeded the uniaxial compressive strength of the grout near the bolt - joint intersection which crushed the grout in this zone. It shows that the value of induced stress in the grout near the shear joint is much higher than the uniaxial strength, and grout in this location can be crushed. The broken sample showed that the grout was crushed around this zone. The damaged area on the upper side of the grout was approximately 60 mm from the shear joint. Figures 33 and 34 show the gap formation after bending in the numerical and laboratory methods respectively. It is noted that the induced stresses were slightly reduced as the pre-tension increased (nearly 10 %). However, it shows they are slightly expanded.

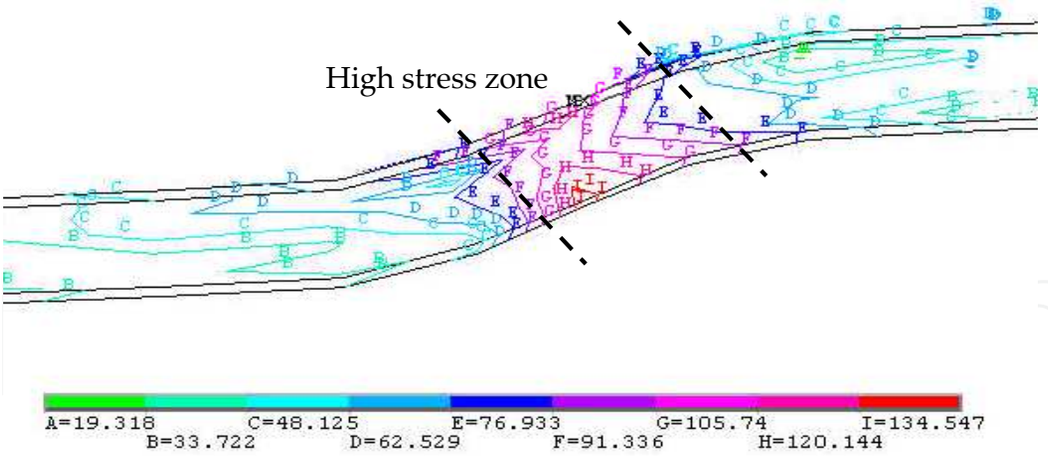

Figure 32. Maximum induced stress contours in grout layer without pre-tension and 20 MPa

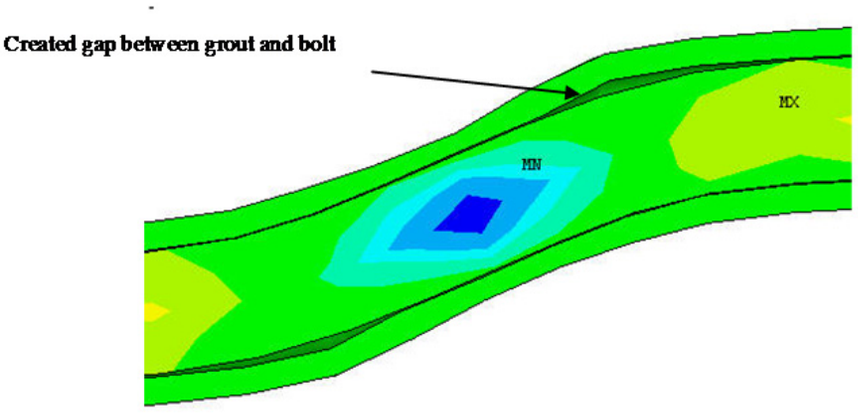

Figure 33. Gap formation in post failure region in 20 MPa concrete in the Numerical simulation

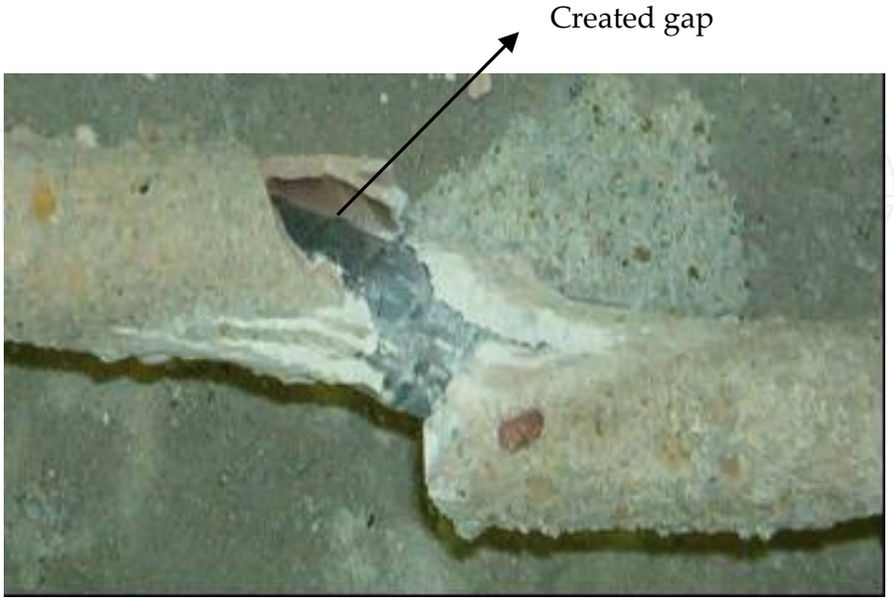

Figure 34. Gap formation in post failure region in 20 MPa concrete in the laboratory test

6.3.2. Strain in grout

While shearing takes place, strains are induced through the grout near the shear joint and reaction zones. The strain in the grout was around ten times greater than the linear region at critical zones. This means that the grout in those areas had broken off the sides that were in tension. The rate of induced strain along the grout in an axial direction is shown in Figure 35.

A comparison of the strain along the joint interface in the grout showed that it decreased between 3% and 5% in the compression and tension zones with increasing pre-tension to 80 kN, which is due to higher shear resistance and lower lateral displacement. It was also found that the grout layer at the bolt - joint intersection will start to crush after slight movement along the joint, which causes plastic strain in the grout layer.

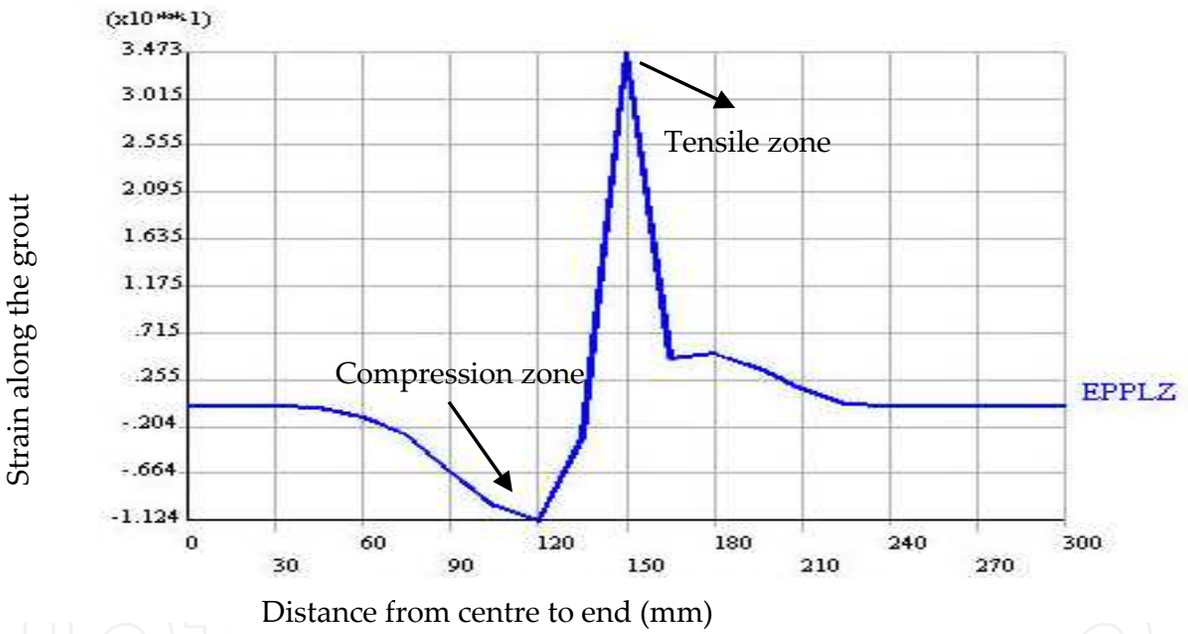

Figure 35. The rate of induced strain along the grout layer without pre-tension in an axial direction

In high strength concrete induced stress was reduced slightly and pre-tension reduces induced stresses along the bolt - grout interface.

From the results at contact pressure in the bolt-grout-concrete it was found that there is an exponential relationship between contact pressure and loading process at the bolt - grout interface, which started after around 15% of the loading process. However, the contact pressure trend in the concrete - grout interface was formed by 2 parts. From the beginning to around 15% of the loading, there is an approximate linear relation followed by an exponential relationship till the end of the load stepping process.

7. Bolt modelling under axial loading

A numerical model was developed to investigate the contact interface behaviour during shearing under pull and push tests. The same 3D solid elements and surface-to-surface contact elements were used to simulate grout and steel. The numerical simulation of the cross section of the bolt and its ribs was complicated, and is almost impossible with the range of software available in the market today. However an attempt was made to model the bolt profile configurations by taking into account the realistic behaviour of the rock - grout and grout - bolt interfaces based on laboratory observations. To achieve this end, the coordinates of all nodes for all materials were defined then all these co-ordinates were inter-connected to form elements, which were extruded in several directions to obtain the real shape of the bolt.

Figure 36 shows the FE mesh. Figure 37 shows the bolt under pull test. Two main fractures were produced as a result of shearing the bolt from the resin. The first one begins at the top of the rib at an angle of about 53^0 running almost parallel to the rib, and the second one has an angle of less than 40^0 from the axis of the bolt. When these fractures intersect they cause the resin to chip away from the main body because it is overwhelmed by the surface roughness of the rib while shearing. Internal pressure produced by the profile irregularities of the bolt induces tangential stress in the grout. The grout fractures and shears when the induced stress exceeds the shearing strength, allowing the bolt to slide easily along the sheared and slikenside fractures in the grout interface.

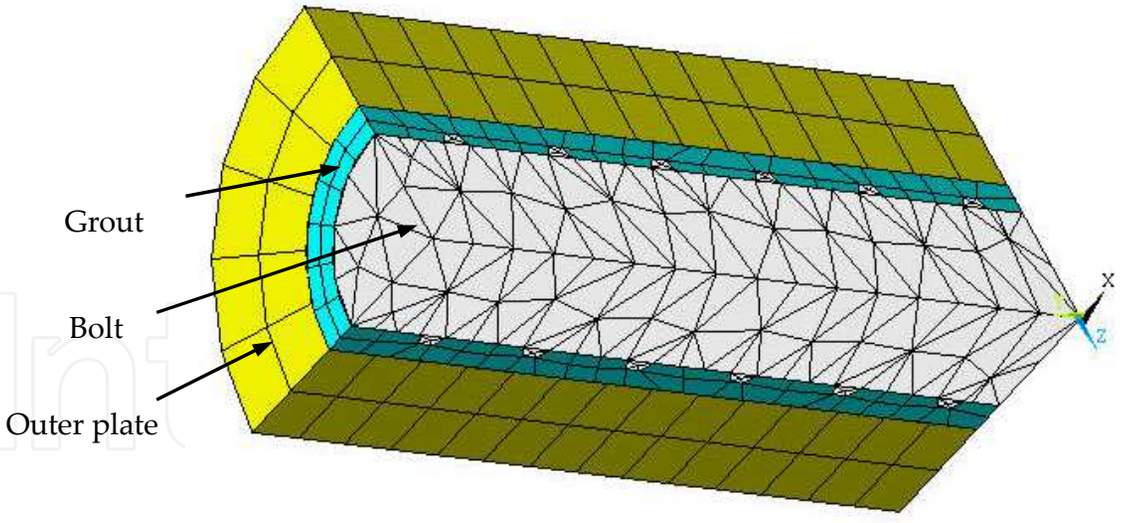

Figure 36. **FE** mesh: a quarter of the model

7.1. Bolt behaviour

From the simulations it was found that there will be an increase in grout - bolt surface de-bonding, and this decrease in diameter due to Poisson's effect in the steel, contributes to an axial elongation of about 0.084 mm at the top collar where the load is applied. This value in push test is around 0.05 mm as shown in Figure 37.

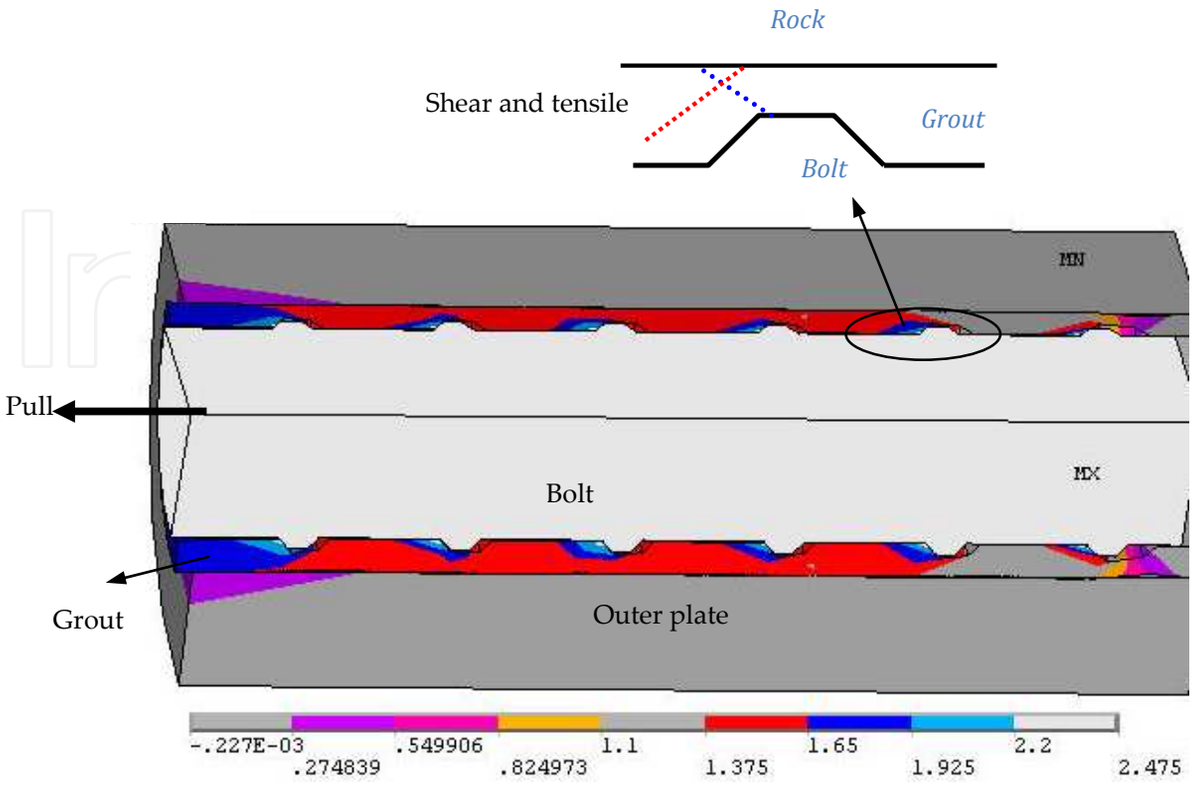

Figure 37. The bolt movement in pulling test

Figure 38 show the maximum induced strain near the applied load position in both the pull and push results. The strain is around the elastic strain and therefore the bolt is unlikely to yield.

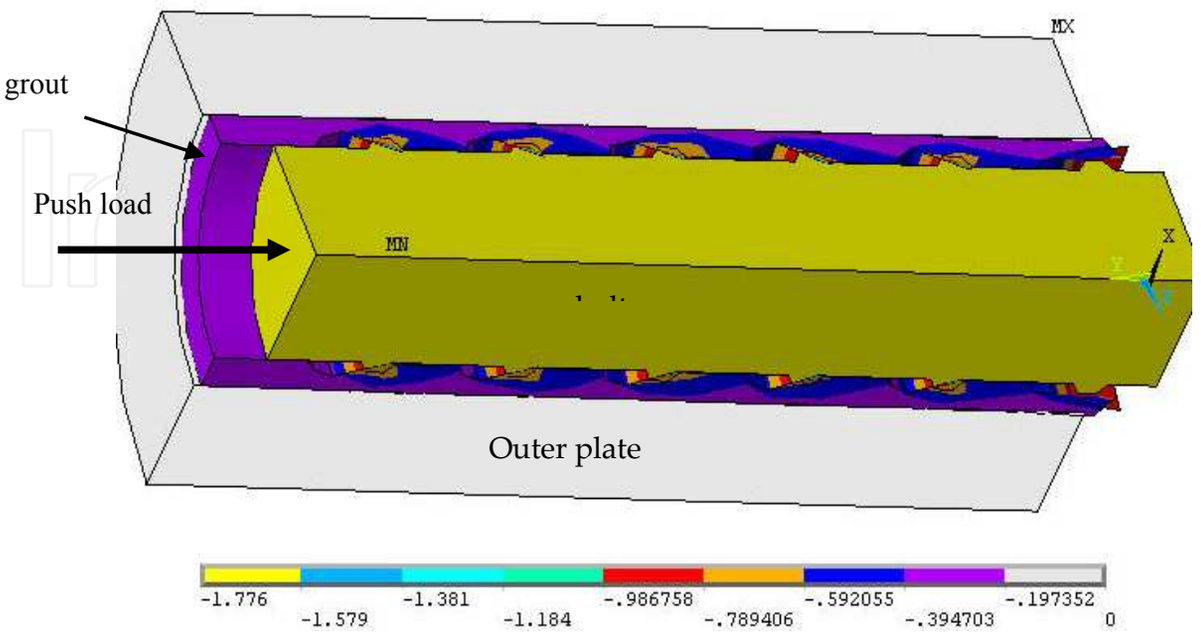

Figure 38. Bolt displacement contour in Bolt Type T1 in case of push test

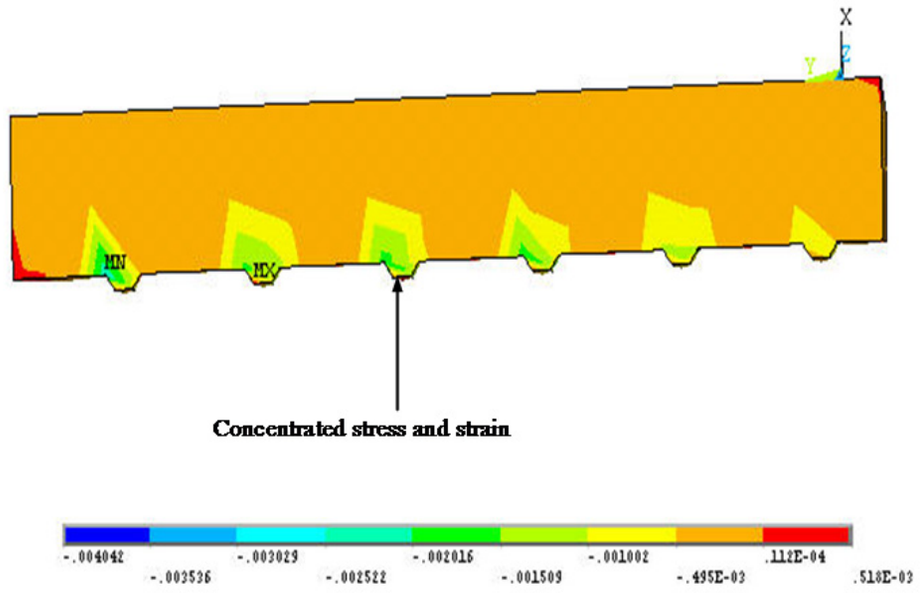

Figure 39. Shear strain in bolt ribs in push test

Maximum tensile stress along the bolt is 330 MPa. This is one half of the strength of the elastic yield point of 600 MPa. This means the bolt behaves elastically and is unlikely to reach a yield situation. Axial stress developed along the bolt is given by:

$$\sigma_t = \frac{4T}{\pi D_b{}^2} \tag{4}$$

and

$$T = \frac{\pi D_b{}^2 * \sigma_t}{4} \tag{5}$$

Where, σ_t is the tensile stress, T is the axial load, D_b is the bolt diameter and σ_y is the yield strength of the bolt. The bolt behaves elastically as long as the following expression is satisfied:

$$\sigma_t < \sigma_y \tag{6}$$

So in this situation with failure along the bolt-grout interface will not yield.

7.2. Grout behaviour

The behaviour of interface grout annulus is assumed to be elastic, softening, residual, plastic flow type. This behaviour was developed by Aydan (1989), and is given as:

$$\tau = G\gamma \quad \tau < \tau_{\max} \tag{7}$$

$$\tau = \tau_{\max} - \frac{\gamma - \gamma_{\max}}{\gamma_r - \gamma_{\max}}(\tau_{\max} - \tau_r) \tag{8}$$

$$\tau = \tau_r \tag{9}$$

where;

- G = Shear modulus of grout interface
- γ = Shear strain at any point in the interface
- γ_r = Shear strain at residual shear strength
- $\gamma_{\max}$ = Shear strain at peak shear strength
- τ_r = Residual shear strength of the interface
- $\tau_{\max}$ = Peak shear strength of interface
- τ = Shear stress at any point in interface

The grout material is in elastic conditions if the following expression is satisfied;

$$T_t < T_y \tag{10}$$

where;

- T_t = Actual bond stress in the grout
- T_y = Yield stress of the grout in shear

From the strain generated along the grout interface it was found that the surface of the grout was disturbed by shear stress induced at the interface and this strain is higher than the elastic strain that damaged the grout at the contact surface. Figure 39 shows the shear stress contour at the grout interface. The whole contact area of the grout was affected by the shear stress and consequently the induced shear strain dominated. The maximum bonding stress was approximately 38% of the uniaxial compressive strength of the resin grout. The stress produced along the grout contact interface was greater than the yield strength of the grout of 16 MPa, and beyond the yield point only a slight increase in load is enough to damage the whole contact surface. Shear displacement increased as a result bonding failure. The shear stress at the bolt - grout interface can be calculated by Equation (11), which agrees with the results from the numerical simulation.

Thus,

$$\tau = \frac{f}{A} = \frac{\sigma \pi D^2}{8\pi r l} = 23.2MPa \tag{11}$$

where;

- τ = Shear stress in the grout - bolt interface (MPa)
- f = Axial force in the bolt (kN)

- A = Contact interface area (mm²)
- D = Bolt diameter (mm)

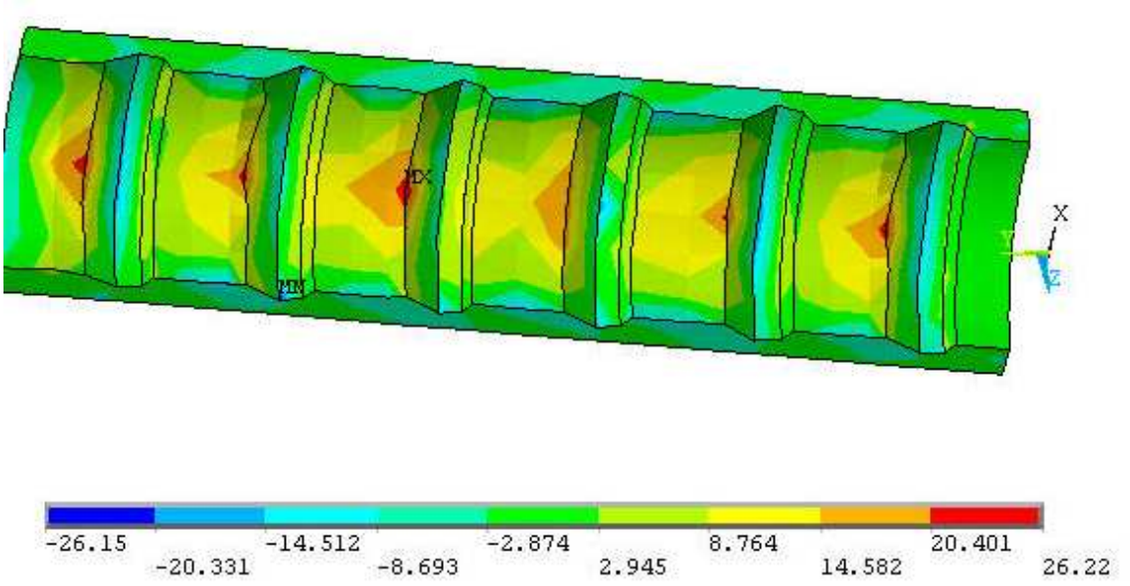

Figure 40. Shear stress contours along the grout interface

Using the *Farmer* (1975) equation the shear strength was equal to 27 MPa.

$$\frac{\tau}{\sigma} = 0.1e^{-(\frac{0.2x}{a})} \tag{12}$$

where;

- τ = Shear stress along the bolt grout interface
- σ = Axial stress
- a = Bolt radius

During shearing the outer plate of the bolt was influenced by the stresses and strains of the resin. From the analyses it was found that induced stress along the surface of the outer plate was insignificant at about 30 % of the yield stress, which is not sufficient to cause the outer plate to yield. In addition, grout de-bonding occurred around 50 to 60 kN at different levels of applied load.

8. Summary

Numerical analysis of the grout – concrete - bolt interaction has demonstrated that:

- There were no significant changes in induced stresses along the bolt with increasing pre-tension load, particularly in the tension zone. However, there was a small reduction in compression stress.
- The yield limit of the bolt at the hinge point depends on the strength of the concrete. In 20 MPa concrete the yield limit was 0.3P and in 40 MPa concrete it increased to 0.4P. A

further increase in the shear force has no apparent influence on stress at the hinges. The distance between the hinge points reduced with increasing strength of concrete.

- The strength of the concrete greatly affects shear displacement and bolt contribution. However, no significant change was observed in the induced stresses beyond the yield point along the axis of the bolt with increasing concrete strength.
- The maximum shear stress was concentrated near the bolt - joint intersection.
- There was an exponential relationship between the shear stress and distance from the shear joint.
- The shear stress was not exceeded during further loading after the yield point. Eventually, a combination of this stress with induced tensile stress at the bolt - joint intersection caused the bolt to fail.
- Shear stress at the bolt - joint intersection increased slightly with an increasing strength of concrete.
- There was no significant change in the hinge point distances with an increase in bolt pre-tension.
- There was a significant increase in shear displacement beyond 35% of the loading step, which is the likely yield point.
- The strain in the shear direction along the concrete was reduced (around 15%) with increasing the pre-tension loading. In both axial and shear directions the strain concentrated near the shear joint.
- The induced stresses exceeded the uniaxial compressive strength of the grout near the bolt - joint intersection, crushing the grout.
- The damaged area in the upper side of the grout was approximately 60 mm from the shear joint.
- Induced stress along the grout was reduced by increasing the pre-tension load nearly 10%. However they have expanded slightly.
- The strain was decreased by around 3% and 5% in the compression and tension zones where the bolt pre-tension load increased to 80 kN.
- Failure of the bolt - resin interface occurred by the grout shearing at the profile tip in contact with the resin.
- Numerical simulation provided an opportunity to better understand the stress and strains generated as a result of the bolt - resin interface shearing. Such an understanding is supported both analytically and by simulation.
- Findings from the experimental test agreed with the numerical simulations and analytical results.

Author details

Hossein Jalalifar
Shaihid Bahonar University of Kerman-Iran

Naj Aziz
Wollongong University- Australia

9. References

[1] Pool.G, Cheng.Y and Mandel.J (2003). Advancing analysis capabilities in Ansys through solver technology. Electronic transactions on numerical analysis 15: 106-121.

[2] Bhashyam.G.R (2002). Ansys Mechanical-A powerful nonlinear simulation tool, 2004. Ansys,Inc. 275 Technology Drive Canonsburge,PA 15317.

[3] Coates.D.F and Yu.Y.S (1970). Three dimensional stress distribution around a cylindrical hole and anchor. Proceeding of 2nd Int. Cong. Rock Mechanics.175-182.

[4] Hollingshead.G.W (1971). Stress distribution in rock anchors. Canadian Geotechnical Journal 8: 588-592.

[5] Aydan.O (1989). The stabilisation of rock engineering structures by rock bolts. Geotechnical Engineering.Thesis. Nagoya, Nagoya**:** 202.

[6] Saeb.S and Amadei.B (1990). Finite element implementation of a new model for rock joints. Int. Symp. of Rock Joints.707-712.

[7] Aydan, O. and T. Kawamoto (1992). Shear reinforcement effect of rockbolts in discontinious rock masses. Int.Sym. of Rock support in mining and underground construction, Canada.483-489.

[8] Swoboda.G and Marence.M (1992). Numerical modelling of rock bolts in interaction with fault system. Int.Sym. of Numerical modelling in Geomechanics.729-737.

[9] Moussa.A and Swoboda.G (1995). Interaction of rock bolts and shotcrete tunnel lining. Int.Sym. of Numerical models in Geomechanics.443-449.

[10] Marence.M and Swobodea. M (1995). Numerical model for rock bolt with consideration of rock joint movements. Rock Mechanics & Rock Enginnering 28.(3): 145-165.

[11] Chen, S. H. and G. N. Pande (1994). Rheological model and finite element analysis of jointed rock masses reinforced by passive, fully-grouted bolts. International Journal of Rock Mechanics and Mining Science & Geomechanics Abstracts 31.(3): 273-277.

[12] Chen, S. H. and P. Egger (1999). Three dimensional elasto-viscoplastic finite element and its application. Int. J. for Numerical and analytical methods in geomechanics 23: 61-78.

[13] Chen, S. H., S. Qiang and S. F. Chen (2004). Composite element model of the fully grouted rock bolt. Rock mechanics and rock engineering 37.(3): 193-212.

[14] Surajit, P. and G. Wije Wathugala (1999). disturbed state model for sand-geosynthetic interfaces and application to pull-out tests. Int. J. for Numerical and analytical methods in geomechanics 23: 1873-1892.

[15] John.C.M and Van Dillen.D.E (1983). Rock bolts: A new numerical representation and its application in tunnel design. Proc.24th U.S. Symp. Rock Mech., Texas A&M University.13-25(Cited in Moosavi 1994).

[16] Peng, S. and S. Guo (1992). An improved numerical model of grouted bolt-roof rock interaction in underground openings. Rock support in mining and underground construction, Canada.67-74.

[17] Stankus.J.C and Guo.S (1996). Computer automated finite element analysis-A powerful tool for fast mine design and ground control problem diagnosis and solving. 5th Conference on the use of computer in the coal industry, West Virginia-USA.108-115.

[18] Fanning, P. (2001). Nonlinear models of reinforced and post tensioned concrete beams. Structural engineering: 111-119.
[19] Feng.P, Lu.X.Z and Ye.L.P (2002). Experimental research and finite element analysis of square concrete column confined by FRP under uniaxial compression. 17th Australian Conference on the Mechanics of Structures and Materials, Gold Coast, Australia.60-65.
[20] Ansys. 2012. Manual.
[21] Cha.E.J, Choi.S.M and Kim.Y (2003). A moment-rotation curve for CFT square column and steel beams according to reliability analysis. Int. Conference on Advances in Structures, Sydney-Australia.943-950.
[22] Hong.S.D, Choi.S.M and Kim.Y (2003). A moment-rotation curve for CFT square columns and steel beams. Int. Conference on Advances in Structures, Sydney-Australia.951-956.
[23] Abedi, K., H. Afshin and A. Ferdousi (2003). Investigation into the behaviour of a novel steel section for concrete filled tubular columns under axial and cyclic loadings. Advances in structures, Australia. 891-897.
[24] Pal.S and Wathugala.G.W (1999). Distribution state model for sand-geosynthetic interfaces and application to pull out tests. Int.J. for Numerical and Analytical Methods in Geomechanics 23: 1873-1892.
[25] Ostreberge. J.O and Gill. S.A (1973). load transfer mechanism for piers. Proceedings of the 9th Canadian rock mechanics symposium, Montreal , Canada, Mines Brance, Departement of Energey, Mines and Resources.235-262.
[26] Nitzsche. R. N and Haas. C. J (1976). Installation induced stresses for grouted roof bolts. International Journal of Rock Mechanics and Mining Science & Geomechanics Abstracts 13.(1): 17-24.
[27] Farmer, I. W. (1975). Stress distribution along a resin grouted rock anchor. Rock mechanics and mining science 12: 347-351.